To link to this article :
URL : http://dx.doi.org/10.1016/j.jnucmat.2008.06.013

Thermodynamic modelling of the plutonium–oxygen system

Christine Guéneau [a],[*], Christian Chatillon [b], Bo Sundman [c]

[a] DEN/DANS/DPC/SCP/LM2T – CEA Saclay, Bat. 450 SE, 91191 Gif-sur-Yvette cedex, France
[b] Laboratoire de Thermodynamique et Physico-Chimie Métallurgiques (UMR 5614 CNRS/UJF/INPG) – ENSEEG, BP 75, 38402 Saint-Martin d'Hères, France
[c] CIRIMAT-INPT, ENSIACET, 118 Route de Narbonne, 30077 Toulouse cedex 4, France

ABSTRACT

The published data for the thermodynamic functions and phase equilibria of the plutonium–oxygen system have been examined. Some inconsistencies have been found for oxygen chemical potential and vaporization data of [$Pu_2O_3 + PuO_{2−x}$] and $PuO_{2−x}$ domains. As the original chemical potential data were not performed at the same temperature and O/Pu ratio, a chart with fixed temperature and composition ranges was built in order to compare all the experimental data. The discrepancies remain difficult to explain. Thermodynamic models of all the phases have been derived by the least-squares minimization procedure using the Thermo-Calc software. The compound energy formalism with the sublattice models $(Pu^{3+}, Pu^{4+})_1(O^{2−}, Va)_2$ and $(Pu^{3+}, Pu^{4+})_2(O^{2−})_3(O^{2−}, Va)_1$ have been chosen to account for the crystal structure, defect chemistry and thermodynamic properties of respectively $PuO_{2−x}$ and $PuO_{1.61}$ phases. The liquid phase was described using the ionic two-sublattice model $(Pu^{3+})_P(O^{2−}, Va^{Q−}, PuO_2, O)_Q$. The reliability of the refined parameters is demonstrated by calculation of the phase diagram, the thermodynamic properties of the phases and the equilibrium partial pressures in the Pu_2O_3–PuO_2 region. Considering the large uncertainties on the experimental information, an overall good agreement was obtained. To improve the thermodynamic description of the system, some missing experimental data are listed.

1. Introduction

This work has formed a part of the FUELBASE project, which is concerned with describing the thermodynamic properties and phase equilibria of the multi-component system U–Pu–O–C–N–Si–Ti–Zr–Mo, which is required for the prediction of the performance of candidate fuels for future nuclear power reactor systems such as (V)HTR (Very High Temperature Reactor), GFR (Gas Fast Reactor) and SFR (Sodium Fast Reactor) systems [1,2]. In fact, nuclear fuel production, fuel behaviour under irradiation and reactor safety analyses of such advanced fuels require an accurate modelling of the thermodynamic data and phase equilibria of these fuel materials. The U–Pu–O–C quaternary is the key system to study mixed oxide (U,Pu)O$_2$ and carbide (U,Pu)C fuels. The objective of the present work is to provide a thermodynamic modelling of the oxygen–plutonium binary system using the CALPHAD method [3].

Considerable efforts have been dedicated to the thermochemical modelling [4,5] and the defect chemistry [6,7] of plutonium oxides. The model of Lindemer and Besmann has been extensively used around the world as reference thermodynamic data for UO$_2$, PuO$_2$ and (U,Pu)O$_2$ fuels [4,5]. However, these models do not allow

describing both thermodynamic and phase diagram data. The liquid and gas phases are not taken into account. The complex region ranging from Pu$_2$O$_3$ and PuO$_2$ is not fully described. A recent assessment has been performed by Kinoshita et al. [8] using the CALPHAD method [3]. However, several features of the phase diagram are not reproduced in this work such as the miscibility gap in the PuO$_{2−x}$ phase and the composition range of the PuO$_{1.61}$ phase. No comparison with experimental information is presented concerning the phase diagram and for the thermodynamic data, only a few experimental values have been used for the oxygen chemical potential data in PuO$_{2−x}$. Finally the model of Kinoshita for the PuO$_{2−x}$ phase, $(Pu)_1(O,Va)_2$, is not compatible with the one that we use in FUELBASE to describe the fluorite fcc phase: $(Pu^{3+}, Pu^{4+}, U^{3+}, U^{4+}, U^{5+}, Zr^{2+}, Zr^{4+})_1(O^{2−}, Va)_2(O^{2−}, Va)_1$ where ionic species are introduced in the sublattices. This ionic multi-sublattice model is chosen to provide a more physically realistic description of the non stoichiometry of the oxide phases related to the defect chemistry where the metal ions, for example, of uranium, can have several valence states +3, +4, +5 as a function of reducing or oxidation conditions. This type of model has been successfully applied to describe the cerium–oxygen [9] and uranium–oxygen [10] systems. A new assessment of the plutonium–oxygen system using the ionic multi-sublattice model for the oxide phases is presented to bring a complete description of the system including the thermodynamic data for all the phases, the phase diagram,

* Corresponding author. Tel.: +33 1 69 08 67 41; fax: +33 1 69 08 92 21.
  E-mail address: christine.gueneau@cea.fr (C. Guéneau).

the oxygen chemical potential and the vapour partial pressure data versus O/Pu ratio and temperature. The thermodynamic parameters of all the phases are derived by the least-squares minimization procedure using the CALPHAD method and the Thermo-Calc software [3]. After a brief review of the literature information on the thermodynamic properties of the Pu–O system and a description of the sublattice models used to describe the phases, the calculated phase diagram and thermodynamic data will be compared to the published data. Finally some calculations on the vaporization behaviour of the Pu–O system will be presented.

2. Survey of literature information

Owing to its great interest for nuclear fuel application, especially (U, Pu)O_2 mixed oxides, the plutonium–oxygen system has been regularly investigated over the past several decades. The phase diagram of the Pu–O system is still subject of controversy. This is due to difficulties related to both plutonium handling and metal–oxygen investigation at high temperature. Priority has been given to the investigation of the oxide part over the metallic part of the diagram. Besides, numerous studies have been undertaken to determine the variation of oxygen potential and partial pressures of the Pu_xO_y gaseous species as a function of O/Pu ratio and temperature in the Pu_2O_3–PuO_2 region which constitute crucial data for fuel application.

The binary system Pu–O contains the gas phase, the liquid phase, the terminal solid solutions based on the six allotropic forms of Pu (α-Pu monoclinic, β-Pu body-centered monoclinic, γ-Pu face-centered orthorhombic, δ-Pu (fcc), δ'-Pu (bct) and ε-Pu (bcc)) and several solid oxide phases. A confusion existed in the literature regarding intermediate phases between the well-known sesquioxide Pu_2O_3 (hexagonal with a small composition range at high temperature, also designated as β-Pu_2O_3 or A phase) and the dioxide PuO_2 (cubic fcc with a composition range from 61.3 to 66.67 at.% O also designated as γ-PuO_{2-x} phase). The intermediate oxide phases are: the oxide $PuO_{1.52}$ (bcc, also designated by cubic Pu_2O_3, α-Pu_2O_3 or C) with a composition very close to the sesquioxide and the oxide $PuO_{1.61}$ (bcc, also designated by α-Pu_2O_3 or C') with a composition range from 61.7 to 63 at.% O. The compound 'PuO' has been subject of controversy. It was reported as a metastable phase by Holley et al. [11] and later included as a stable compound with a congruent melting at about 2173 K in the phase diagram of Chikalla et al. [12]. Martin who performed some melting tests on Pu–Pu_2O_3 mixtures did not observe the 'PuO' compound in the quenched microstructures of the samples [13]. This compound was finally recognized to be metastable in the review of Wriedt [14] and is thus not taken into account in the present work. The crystallographic data on the phases of the system Pu–O are listed in Table 1.

Table 1
Crystallographic data on the phases of the Pu–O system

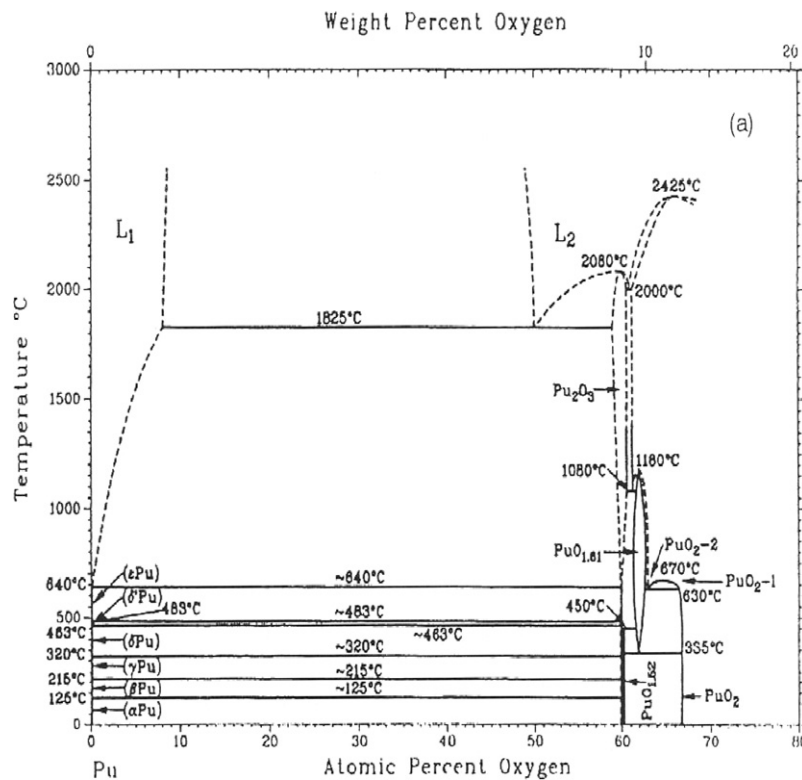| Phase	Lattice parameters (nm)	Space group	Author reference
α-Pu	$a = 0.6183(1)$, $b = 0.4822(1)$, $c = 1.0963(1)$ $\beta = 101.79°$	$P2_1/m$	[15]
β-Pu	$a = 1.1830$, $b = 1.0449$, $c = 0.9227$ $\beta = 138.65°$	$C2/m$	[16]
γ-Pu	$a = 0.31587(4)$, $b = 0.57682(4)$, $c = 1.0162(2)$	$Fddd$	[17]
δ-Pu	$a = 0.46347$	$Fm\bar{3}m$	[18]
δ'-Pu	$a = 0.3339(3)$, $c = 0.4446(7)$	$I4/mmm$	[18]
ε-Pu	$a = 0.36375$	$Im\bar{3}m$	[18]
Pu_2O_3	$a = 0.3838(1)$, $c = 0.5918(1)$	$P\bar{3}m1$	[19]
$PuO_{1.52}$	$a = 1.1045$	$Ia\bar{3}$	[20]
$PuO_{1.61}$	$a = 1.0991$	$Ia\bar{3}$	[21]
PuO_2	$a = 0.53955$	$Fm\bar{3}m$	[22]

Fig. 1. Pu–O phase diagram from Wriedt's critical analysis [14].

2.1. Phase diagram

With time, successive versions of Pu–O phase diagrams have been published by Holley et al. [11], Chikalla et al. [12], Gardner et al. [23] Sari et al. [21], Dean et al. [24], Boivineau [20] and Besmann [25], based on experimental work. In 1990, Wriedt proposed a phase diagram based on an extensive critical analysis of all previous experimental studies [14]. The resulting phase diagram of Wriedt adopts the phase boundaries proposed by Sari et al. [21] and Besmann [25] in the Pu_2O_3–PuO_2 region. The Pu-rich boundary of PuO_{2-x} at higher temperature is based on the data of Messier [26] and Ohse et al. [27]. The Pu–Pu_2O_3 region, very uncertain, is based on the experimental work of Martin et al. [13]. In our work, we have adopted the selected experimental data on phase diagram coming from the critical analysis of Wriedt for the least-squares minimization procedure (Fig. 1). The phase equilibria are described and a brief review of the experimental information is presented.

2.2. Pu–Pu₂O₃ region

In the metal–oxide region, the experimental data are rare. At low temperature, the sesquioxide Pu_2O_3 (hexagonal) is found to be in equilibrium with plutonium by Holley et al. [11] with a very small solubility of oxygen in Pu (25 ± 10 ppm) from 1273 to 1423 K. At high temperature, the miscibility gap in the liquid state is based on the melting experiments of Martin et al. [13]. According to the authors, the monotectic reaction [Liquid2 (O/Pu ~ 1) = Liquid1 (O/Pu ~ 0.1) + Pu_2O_3] occurred at 2098 ± 40 K [13]. These results on Pu–O system are consistent with the existence of a miscibility gap in the liquid state in both U–O and U–Pu–O systems [13]. As indicated in the phase diagram of Wriedt [14], there is no data on the oxygen solubility limit in liquid plutonium at high temperature.

2.3. Pu₂O₃–PuO₂ region

This region has been extensively investigated at temperatures below 1500 K. The $PuO_{1.52}$ compound was first observed by Holley et al. [11] to be in equilibrium with both Pu_2O_3 (hexagonal) and PuO_2 up to ~2173 K. Later, Gardner et al. [23] confirmed the existence of this phase with a O/Pu ratio of 1.515 in equilibrium with both $PuO_{1.98}$ and Pu_2O_3 (hexagonal) up to ~573 K. At 623 K, the $PuO_{1.515}$ compound was found to decompose into Pu_2O_3 (hexagonal) and $PuO_{1.61}$(cubic). A two-phase region ($PuO_{1.515}$ + $PuO_{1.61}$) was assumed to exist from ~573 to ~623 K. These phase boundaries at low temperature have been adopted in the phase diagrams published by Sari et al. [21] and Wriedt [14].

For the $PuO_{1.61}$ cubic phase, some uncertainties remained for a long time on the fact whether it was or not a separate phase from $PuO_{1.52}$ and PuO_2. The stability range in temperature and composition were also not clearly established. It has been fixed by Sari et al. [21] from heat treatments and X-ray diffraction experiments for $T < 1300$ K. The $PuO_{1.61}$ phase was found to be stable above ~573 K where it decomposed into $PuO_{1.52}$ and $PuO_{1.995}$ (instead of $PuO_{1.98}$ from Gardner et al. [23]). The phase was found to exhibit an extended homogeneity range from O/Pu = 1.61 to 1.69 instead of being a stoichiometric compound according to Chikalla et al. [12] and Gardner et al. [23]. The phases $PuO_{1.61}$ and PuO_{2-x} were observed to be in equilibrium from 573 K to ~900 K. This two-phase domain replaced the large miscibility gap in the fcc PuO_{2-x} phase reported by Chikalla et al. [12] and Gardner et al. [23]. According to Sari et al. [21], the resulting miscibility gap in the fcc phase existed in a narrow temperature range above 900 K according to the monotectoid reaction [PuO_{2-x} (O/Pu $\sim$ 1.7) = $PuO_{1.98}$ + $PuO_{1.62}$]. The consistency of the modified phase diagram with the EMF data of Markin et al. [28] was verified by

Sari et al. [21]. In another X-ray diffraction study, Boivineau et al. [20] confirmed the main features of the phase diagram of Sari et al. A very small second miscibility gap in the cubic PuO_{2-x} phase was found to exist for a O/Pu ratio close to 1.75 and at $T \sim 1000$ K. The existence of this very small miscibility gap instead of a two-phase domain [$PuO_{1.61}$ + PuO_{2-x}] has to be confirmed and consequently it is not taken into account in [14] and in the present work.

The phase equilibria in the Pu_2O_3–PuO_2 region at temperatures between 1400 and 1600 K were investigated by Besmann from measurements of CO equilibrium pressures over oxide–graphite mixtures [25]. PuO_{2-x} (fcc), $PuO_{1.65}$ (bcc) and $PuO_{1.5}$ (hexagonal) were observed exhibiting a significant homogeneity range. The results of Besmann argue for the high temperature $PuO_{1.62}$ (bcc) phase, reported by Chikalla et al. [12], Gardner et al. [23] and Riley et al. [29], to be the lower phase boundary of PuO_{2-x} (fcc) instead of being a separate phase. The author explained the previous results by the difficulties related to the quenching of the PuO_{2-x} phases from high temperatures. The results obtained by Besmann are in good agreement with the previous investigations on the vaporization behaviour of the system Pu_2O_3–PuO_2 at high temperature carried out by Messier [26] and Ohse et al. [27], which indicated the wide homogeneity range of PuO_{2-x} over ~1.6 < O/Pu < 2 from 1650 K to 2380 K. From the analysis of the variation of oxygen equilibrium pressures versus temperature and composition, the eutectoid reaction [PuO_{2-x} (fcc) with $x \sim 0.395 = PuO_{1.5}$ (hex) + $PuO_{1.65}$(bcc)] was assumed to occur at $T < 1400$ K by Besmann [25]. In addition, a congruent decomposition of fcc PuO_{2-x} phase into bcc $PuO_{1.65}$ phase was assumed to occur around 1450 K but the exact temperature could not be accurately determined.

As indicated in the phase diagram of Wriedt [14], the solidus and liquidus curves between Pu_2O_3 and PuO_2 remain uncertain. Melting temperatures of oxides with compositions between Pu_2O_3 and PuO_2 were determined by Chikalla et al. [12] under helium by thermal analysis. Pu_2O_3 (hexagonal) and $PuO_{1.62}$ (designated as α'-Pu_2O_3 cubic) were reported to melt congruently at, respectively, 2358 ± 25 K and 2633 ± 20 K. The uncertainty on the measured liquidus temperature for PuO_2 is high due to the oxygen loss by vaporization at high temperature leading to a substoichiometric composition: a minimum temperature of 2553 ± 30 K is found for O/Pu = 1.62 starting from PuO_2. The melting point of PuO_2 could not be measured by Chikalla et al. [12] and was indicated at 2673 K according to the measurements of Russel [30]. A eutectic reaction has been arbitrarily drawn between Pu_2O_3 (hexagonal) and α'-Pu_2O_3 at 2303 K. Riley [29] determined the liquidus temperatures for compositions in the Pu_2O_3–PuO_2 range using flame melting in oxidizing atmosphere for PuO_2 or electric arc with imposed oxygen pressures (using argon/oxygen gas mixtures). The author proposed a congruent melting point for $PuO_{1.62}$ at 2473 ± 20 K, an eutectic reaction [liquid = Pu_2O_3 + $PuO_{1.62}$] at 2243 ± 5 K and a minimum in the liquidus curve for $PuO_{1.8}$ meaning that an azeotropic composition would exist. The measurements of Chikalla et al. [12] for $PuO_{1.62}$ are discarded in this work because $PuO_{1.62}$ is not a high temperature phase as shown by Besmann [25] and the values seem to be too high compared to the measurements of Riley [29].

2.4. PuO₂–O region

Uncertainties still remain on the existence of a possible hyperstoichiometric PuO_{2+x} domain. Oxidation heat treatments with an excess of oxygen were tentatively performed in order to analyze the existence of a possible PuO_{2+x} domain. Experiments by Holley et al. [11], Riley [29] and Drummond et al. [31] led to O/Pu ratio higher than 2. A O/Pu ratio equal to 2.01 ± 0.008 at 1143 K was determined using gravimetry in [31]. Jackson and Rand [32] showed that the excess of oxygen was due to the adsorption of

oxygen at the surface as a function of O_2 pressure and specific surface. Haschke et al. [33] reported the formation of PuO_{2+x} when $PuO_2(s)$ was stored in presence of water according to the reaction $[PuO_2(s) + H_2O(g) = PuO_{2+x}(s) + H_2(g)]$. On the basis of hydrogen volumetric measurements, the authors estimated the Gibbs energy of PuO_{2+x} which would exist up to O/Pu = 2.5 [33]. Neck et al. [34] estimated the enthalpy of formation of Pu_4O_9 and PuO_3 from data on neptunium and uranium oxides as well as actinyl and hydroxides phases. The authors reported that the Gibbs energy values estimated by Haschke et al. [33] for PuO_{2+x} were in error by at least 85–160 kJ/mol for $PuO_{2.25}(s)$. Martin et al. [35] confirmed by X-ray absorption spectroscopy that the oxidation degree is the one of $PuO_2(s)$ (no formation of Pu^{5+}) for PuO_2 samples ignited or treated under water vapour. Farr et al. [36] identified $Pu(OH)_4$ or some Pu(V) phases using XPS analysis on hydrated plutonium oxides. But after dehydration, the PuO_2 compound was recovered without any shift of the analyzed band. These features have been confirmed by Conradson et al. [37] using X-ray absorption. First-principle calculations were performed by Petit et al. [38] and Korzhavyi et al. [39] to determine the stability of the PuO_{2+x} phases or higher plutonium oxides. The two investigations are not consistent on the variation of the lattice parameter of the PuO_{2+x} phase with oxygen content. Petit et al. [38] predicted a decrease of the lattice parameter with oxygen meanwhile Korzhavyi et al. [39] proposed an increase in agreement with the experiments of Haschke et al. [33]. Korzhavyi et al. [39] proposed a new mechanism to explain hydrogen production based on an increasing yield of water radiolysis when it is absorbed on the PuO_2 surface.

In view of all these studies on the behaviour of PuO_2 under water pressure, the existence of an hyperstoichiometric domain for PuO_2 is not yet proved. If existing, the deviation from the stoichiometry may be small according to the thermogravimetric analysis of Drummond et al. [31] that led to O/Pu < 2.01 ± 0.008. Thus the possible hyperstoichiometric domain of PuO_2 is not taken into account in the present work.

The selected experimental data for the phase diagram are reported in Table 2.

This review of the experimental information on the Pu–O phase diagram allows pointing out the lacking data for which new measurements would be helpful to definitely fix the phase diagram. The knowledge of the Pu–Pu_2O_3 region could be improved by bringing new experimental data on the oxygen solubility limit in liquid plutonium, the boundaries of the liquid miscibility gap, the liquidus and solidus temperatures for [Pu_2O_3/liquid] equilibrium and the composition range of hexagonal Pu_2O_3 phase. In Pu_2O_3–PuO_2 region, experimental work on the liquidus and solidus temperatures, the plutonium rich boundary of the PuO_{2-x} phase, the decomposition temperature of the $PuO_{1.61}$ phase and the critical temperature of the miscibility gap in the fcc PuO_{2-x} phase would be helpful.

2.5. Thermodynamic data

The experimental data from the literature on the thermodynamic properties of the phases are briefly reviewed.

2.5.1. Compounds

Thermodynamic data exist mainly on Pu_2O_3 and PuO_2 compounds. For the Pu_2O_3 compound, determinations of the heat capacity at low temperature by Flotow et al. [41] (including a λ transition at 17.65 K) led to an entropy value at 298 K as compiled by Glushko et al. [42] and Lemire et al. [43] and retained in the SGTE data bank [44]. Heat capacity data are available only up to 350 K. Glushko estimated the high temperature heat capacity by comparison with $PuO_2(s)$ (using a C_p ratio ≈ 1.7 from 350 K to the melting temperature 2358 K). The enthalpy of formation has been

Table 2
Experimental database for the Pu–O system

Data	Temperature range (K)	Composition range (O/Pu)	Phases	Reference
Phase diagram	2100	0–1.5	L1, L2, Pu_2, O_3	[13]
Phase diagram	600–2700	1.5–2	$PuO_{1.61}$, PuO_2, L	[12]
Phase diagram	2200–2700	1.5–2	Pu_2O_3, PuO_2, L	[29]
Phase diagram	500–1300	1.5–2	Pu_2O_3, $PuO_{1.61}$, PuO_2	[20]
Phase diagram	500–1000	1.5–2	Pu_2O_3, $PuO_{1.52}$, $PuO_{1.61}$, PuO_2	[23]
Phase diagram	600–1400	1.62–2	Pu_2O_3, $PuO_{1.61}$, PuO_2	[21]
Phase diagram	1400–1600	1.4–1.9	Pu_2O_3, $PuO_{1.61}$, PuO_2	[25]
Phase diagram	2700	2	PuO_2	[30]
Phase diagram	2100–2400	1.5–1.9	Pu_2O_3, PuO_2	[26]
Phase diagram	1800–2200	1.5–2	Pu_2O_3, PuO_2	[27]
Phase diagram	2718	2	PuO_2	[40]
Enthalpy of formation, entropy	298.15	1.5–2	Pu_2O_3, $PuO_{1.52}$, $PuO_{1.61}$, PuO_2	[43]
Partial oxygen enthalpy	1373	1.5–1.99	Pu_2O_3, $PuO_{1.61}$, PuO_2	[46]
Partial oxygen Gibbs energy	1073–1573	1.98–2	PuO_2	[56]
Equilibrium oxygen pressure	1400–1600	1.4–1.8	Pu_2O_3, $PuO_{1.61}$, PuO_2	[25]
Partial oxygen Gibbs energy	1273–1473	1.77–2	PuO_2	[55]
Partial oxygen Gibbs energy	1023	1.54–2	Pu_2O_3, $PuO_{1.61}$, PuO_2	[45]
Partial oxygen Gibbs energy	1750–2250	1.7–1.9	PuO_2	[60]

derived at different temperatures from high temperature measurements of oxygen partial Gibbs energy [25,45] or partial enthalpy [46]. Glushko retained the mean value of the two sets of data [25,45], and calculated the standard enthalpy of formation using their free energy function calculated from the above estimated heat capacity.

Concerning PuO_2, numerous data are available. Calorimetric measurements have been undertaken by Sandenaw [47] on $^{239}PuO_2$ specimen between 15 and 325 K and by Kruger and Savage [48] from 192 to 320 K. Additional measurements were performed on less radioactive specimen of $^{242}PuO_2$ and $^{244}PuO_2$ from 12 to 350 K by Flotow et al. [41]. In these plutonia specimen, the irradiation effects are less important and the measurements are thus more accurate than in the previous studies. The heat capacity of PuO_2 at high temperature has been measured from 300 to 1100 K by Engel [49]. The enthalpy increments were determined from 298 to 1404 K by Kruger and Savage [48], from 1500 to 2715 K by Ogard [50] and from 353 to 1610 K by Oetting [51]. The data of Ogard suggest a sharp increasing of the heat capacity above 2370 K. This feature was attributed to either a partial melting of PuO_2 or to the interaction of the oxide with the tungsten crucible [51]. Furthermore, the high oxygen potential of stoichiometric PuO_2 may lead to the formation and vaporization of gaseous tungsten oxides and the additional gas condensation enthalpy could explain the increasing of the measured enthalpy increments. However, as this type of behaviour has been observed for ThO_2, UO_2 and ZrO_2, the heat capacity increase could be also attributed to the formation of Frenkel and Shottky defects at high temperature [52]. For the enthalpy of formation of PuO_2, there is a good agreement between the values obtained by calorimetry by Popov et al. [53], Holley et al. [11] and Johnson et al. [54].

Concerning the intermediate oxide phases, there is no direct measurement of thermodynamic data. For the $PuO_{1.61}$ phase, the enthalpy of formation has been estimated from experimental

oxygen potentials measurements at high temperature [45,46]. There are no experimental data on the $PuO_{1.52}$ compound. Some thermodynamic data on both $PuO_{1.52}$ and $PuO_{1.61}$ have been estimated in [8,43].

2.5.2. Oxygen partial Gibbs energies

Numerous experimental data are available on the variation of the partial Gibbs energy of O_2 as a function of temperature and O/Pu ratio in PuO_{2-x} composition range. Several experimental methods have been used: E.M.F. by Markin et al. [28,45] and Woodley [55], thermogravimetry by Swansson [56], Woodley [55] and Sorensen [57] using different gas mixtures, electrical conductivity measurement by Atlas et al. [58] under controlled oxygen potential using (H_2/H_2O) mixture, CO pressure measurements over {oxide + graphite} mixtures by Besmann [25], heterogeneous CO/ CO_2 equilibrium by Kent et al. [59] and transpiration with H_2/ H_2O flow by Tetenbaum [60]. Some important discrepancies can be found between the different sets of experimental data as reported by Besmann and Lindemer [5] and no explanations for these discrepancies have been given. But as the experiments were not performed at the same temperatures and O/Pu ratios, a direct comparison is difficult. In order to compare all these original data, it is necessary to scale them in a common chart as already done by Labroche et al. [61] and Baïchi et al. [62] for the critical analysis of the U–O system. Depending on the way experiments are performed, two types of representations are possible in order to compare directly these data: $\mu(O_2)$ versus $\log 10(x)$ at fixed temperatures and $\mu(O_2)$ versus temperature for fixed O/Pu ratios. The data sets of each author have been fitted to build a chart of data recalculated for fixed temperatures ranging from 1100 to 2100 K and fixed O/Pu ratios from 1.7 to 1.995 in order to compare the different sets of data in the same conditions of temperature and O/Pu ratio. A comparison between the calculated oxygen potential and the chart of data recalculated from the data of the literature is presented in Section 4. The new chart of data shows that the oxygen chemical potential data of Woodley [55] are systematically lower than the other sets of data whereas the measurements of Markin et al. [45] are the highest values. Some intermediate results were measured by Swansson [56]. The values obtained by Kent et al. [59] and Atlas et al. [58] are consistent with those of Markin et al. [45]. The discrepancy between the lowest [55] and highest [45] values can reach 100 kJ/mol at 1200–1300 K. At low temperature (1000–1300 K), a reason for these discrepancies can be related to the difficulties to reach the equilibrium during the experiments, especially due to small chemical potential differences when approaching the miscibility gap. At 1500 K, the deviation between the experimental data has decreased to less than 5 kJ/mol. At temperatures above 1600 K, the experimental data are scarce. The data of Woodley [55] are usually considered as good values because the author has used two different experimental methods, thermogravimetry and E.M.F. which lead to consistent results. This only means that for the same composition the two oxygen potentials are similar and consequently any discrepancy should come from the composition uncertainty. But it does not explain such large discrepancies with the other authors who have in such cases used the same experimental methods (E.M.F. for Markin et al. [45], thermogravimetry for Swansson [56]). The uncertainty on the O/Pu ratio is certainly the most important one to consider. The values of the uncertainties on the O/Pu ratios, $\Delta G(O_2)$ and temperature when reported by the different authors do not explain such large discrepancies. Besmann et al. [5], Nakamura [6], Stan et al. [7] who modelled the thermochemical properties of plutonia have either taken into account all the experimental data or have selected some of them without any explanation. Facing the lack of any evidence in the experimental errors, we have selected the following data for the optimization (Table 2): Markin at 1023 K [28],

Swansson at 1073, 1173, 1273, 1370, 1469, 1569 K [56], Woodley at 1273, 1373, 1473 K [55], Besmann at 1400, 1500, 1610 K [25], Tetenbaum at 1750, 2050, 2250 K [60].

2.5.3. Oxygen partial enthalpies

Two sets of experimental data are available for the partial enthalpy of O_2 at 1373 K versus O/Pu ratio from oxygen dissolution calorimetry measurements performed by Dean et al. [24] and Chereau et al. [46]. Differences exist between these two sets of values published by the same team and measured with the same apparatus. The data published by Chereau et al. are by about 50 kJ/mol lower ($\sim$5%). According to Chereau et al. [46], this change is due to the improvement of the experimental conditions in order to decrease the scattering of the data. This type of calorimetric method is very difficult to carry out as it requires measuring a few joules increment which necessitates a very good interpolation of the base lines at the beginning and the end of each thermal effect. An error of 7% can be attributed to these data. Chereau et al. [46] proposed an explanation of the variation of the oxygen partial enthalpy versus O/Pu ratio in relation with the phase diagram: (i) the partial enthalpy plateau from O/Pu = 1.5–1.6 may correspond to the $[Pu_2O_3 + PuO_{1.61}]$ domain, (ii) the partial enthalpy curve ranging from 1.61 to 1.7 may be the $PuO_{1.61}$ single-phase domain; (iii) the narrow partial enthalpy plateau between O/Pu = 1.61 and 1.71 would characterize a two-phase domain $[PuO_{1.61} + PuO_{2-x}]$; (iv) the smooth partial enthalpy curve for O/Pu > 1.71 may correspond to the extended PuO_{2-x} composition range. The same curve was found for two different samples. The shape is very complex especially in the assumed $PuO_{1.61}$ single phase domain. If realistic, this curve may be reproduced by considering a complex structure of defects in this phase. Conversely the complex evolution could be due to kinetic effects not entirely included in the thermal effect observed by the calorimeter within a reasonable time (about 10–20 min). Indeed, such effects were proposed for the quite strange evolution of the partial oxygen enthalpy in the UO_{2+x} compound [62] close to the stoichiometric composition. As indicated in Table 2, the data of Chereau et al. [46] have been considered for the optimization.

2.5.4. Vapor pressure measurements

For the two-phase domain Pu_2O_3–PuO_{2-x} (and diphasic Pu_2O_3– $PuO_{1.62}$ domain), total pressure measurements were performed using the Knudsen method either in reducing conditions by Phipps et al. [63] and Ackermann et al. [64], or starting from well known compositions by Messier [26] and Ohse et al. [27] assuming that PuO(g) is the major constituent in the gas phase. With this assumption for the composition of the gas phase, the pressure measurements of Ackermann et al., Ohse et al. and Phipps et al. are in good agreement. Only the pressure data of Messier [26] are slightly lower. Using mass spectrometry, Battles et al. [65] confirmed that PuO(g) is the major species in the gas phase in equilibrium with Pu_2O_3–PuO_{2-x} (2 − x = 1.61) phases but $PuO_2(g)$ and Pu(g) were also detected and pressure laws for $PuO_2(g)$, PuO(g) and Pu(g) were proposed.

Ackermann et al. [64] deduced the Gibbs energy of formation of PuO(g) from their pressure measurements and using the thermodynamic functions of the condensed phases Pu_2O_3 and $PuO_{1.62}$ reported in [45]. In the compilation of Glushko et al. [42], the thermodynamic properties of PuO(g) were calculated from molecular parameters (spectroscopic investigations) and from the present total measured pressures using their retained data for Pu_2O_3(s).

For measurements above plutonia, total vapour pressures have been measured by Mulford et al. [66], Ohse et al. [27], Messier [26] and Ackermann et al. [64] using the Knudsen effusion method. In more recent mass spectrometric studies, Battles et al. [65] and Kent [67] measured the partial pressures of PuO(g) and $PuO_2(g)$ above

plutonia. There is no detailed information concerning the experimental conditions on the work performed by Kent [67] who only gave equations for the partial pressures. Ackermann et al. observed a congruent vaporization for O/Pu = 1.92 ± 0.03 at 2025 K. Using the assumption that the vapour was almost entirely constituted of PuO$_2$(g) (a small correction of 9% PuO(g) was applied), and from the data of Markin et al. for the thermodynamic functions of PuO$_{1.92}$(s) [45], Ackermann et al. determined the Gibbs energy of formation of PuO$_2$(g). This thermodynamic analysis allowed calculating the partial pressures of all the gaseous species as a function of temperature and O/Pu ratio as well as the congruent composition for PuO$_{2-x}$ in both closed and open systems (effusion cells). The reported congruent composition at 2000 K in an open system is of 1.85 whereas the measured value is equal to 1.92. Conversely, other experimental data in open systems led to a congruent composition in the range 1.84–1.89 for 1800–2200 K from Ohse et al. [27], 1.81–1.87 for 2080–2380 K from Messier [26], 1.83 at 2230 K from Battles et al. [65]. The value 1.92 measured by Ackermann et al. disagrees significantly from other experimental data [28]. To explain such a deviation, the problems related to the quenching conditions of the specimen from high temperature can be mentioned as well as the post experimental composition analysis. The method may suffer from adsorption phenomena during the excess oxidation step before reduction by CO and the uncertainties are difficult to verify. Concerning the pressure measurements, most of the authors assumed that PuO$_2$(g) is the major gas species above congruent PuO$_{2-x}$. Assuming PuO$_2$(g) as the major gas constituent, the total measured pressures by effusion performed by Ackermann et al., Ohse et al., Messier, Mulford et al., Battles et al. and Kent are in good agreement.

Concerning the partial pressure measurements above congruent plutonia using mass spectrometry, the investigations performed by Battles et al. [65] and Kent [67] lead to closed values for PuO(g) and PuO$_2$(g) partial pressures but the authors are not in agreement concerning the major species in the vapour phase. For Battles, PuO(g) is the major constituent whereas Kent found a higher partial pressure for PuO$_2$(g). Thus, further studies would be necessary to perform in order to clarify the situation concerning the partial pressure measurements in the vapour. The agreement for the congruent composition and the measured total pressures is good compared to previous studies since the mass loss in the effusion method was also used for calibrations in conjunction with the mass spectrometer. Thus, the differences between Battles et al. and Kent partial pressures may come from the choice of mass spectrometric parameters (ionisation cross sections and their estimates).

In the compilation performed by Glushko et al. [42], molecular parameters for PuO$_2$(g) come from spectroscopic data associated with estimates. Formation enthalpy is then deduced from the mean value of sublimation enthalpy of PuO$_2$(s) into PuO$_2$(g) as measured for the congruent compositions and their free energy function. The congruent solid is taken as PuO$_2$(s).

By analogy with UO$_3$(g) the gaseous species PuO$_3$(g) has been considered by Krikorian et al. [68] in transpiration experiments and detected by Ronchi et al. [69] using mass spectrometry. The authors have derived a formation enthalpy for the PuO$_3$(g) molecule at 298.15 K: −562.8 ± 5 kJ/mol according to Krikorian et al. [68] and −621 kJ/mol by Ronchi et al. [69]. In the transpiration experiments of Krikorian et al. [68], the measurements seem to be inaccurate as the PuO$_3$(g) molecule is reported to react with the silica wool during the tests. The evaluation made by Ronchi et al. [69] seems to be also uncertain as the calculation was performed on the basis of estimated data for the oxygen potential and from the ratio of the ionic intensities (PuO$_2^+$/PuO$_3^+$) arbitrarily corrected for 50% PuO$_2^+$ fragment contribution coming from PuO$_3$. The two values of formation enthalpy for PuO$_3$(g) are not in good

agreement. If the value of Ronchi et al. [69] was correct, Krikorian et al. [68] would have observed much larger quantities of PuO$_3$(g) in the transpiration experiments. Thus the contribution of the PuO$_3$(g) that may be quite low is not taken into account in the present modelling of the gas phase for the Pu–O system. The present experimental pressure data have not been used in the optimization. But the pressures calculated using our modelling for the condensed phases and using the thermodynamic data estimated by Gluhko et al. [42] for the gaseous species will be compared to all these experimental data in Section 4.

3. Thermodynamic modelling

The PARROT module of the Thermo-Calc software was used for the optimization procedure [70,71]. The oxygen solubilities in the different allotropic forms of plutonium are neglected. Pu$_2$O$_3$ and PuO$_{1.52}$ are treated as stoichiometric compounds. The assumed departure from stoichiometry of Pu$_2$O$_3$ at high temperature is not taken into account. The Gibbs energy functions of all the phases are referred to the enthalpy of the pure elements in their stable state at room temperature 298.15 K and 1 bar ($^\circ H_i^{SER}(298.15$ K)).

3.1. Pure elements

The Gibbs energy functions of the pure elements i at temperature T and in their structural state φ $G_i^\varphi(T)$ are given by

$$G_i^\varphi(T) - {}^\circ H_i^{SER}(298.15 \text{ K}) = a + bT + cT\ln T + \sum d_n T^n \quad (1)$$

where n is an integer (2, 3, −1, ...). In the present work, the parameters reported by Dinsdale are used for pure plutonium and oxygen data [72].

3.2. Pu$_2$O$_3$ and PuO$_{1.52}$ stoichiometric compounds

For these compounds, the Gibbs energy function has the same form as in Eq. (1):

$$G^\varphi(T) - \sum_i n_i^{\varphi\circ} H_i^{SER}(298.15 \text{ K}) = a + bT + cT\ln T + \sum d_n T^n \quad (2)$$

where n_i^φ is the number of atoms of each element i in the oxide formula.

For the PuO$_{1.52}$ compound, heat capacity data reported by Kinoshita et al. [8] corresponding to c and d_n coefficients, were used. For the Pu$_2$O$_3$ compound, the Gibbs energy function from the SGTE substance database [44,42] has been taken as initial parameters. For both compounds, the coefficients a and b are optimized in the present work.

3.3. PuO$_{2-x}$ fcc phase

PuO$_2$ adopts the fluorite structure like UO$_2$ which is typical of ionic compounds. In the present work, the model for PuO$_2$ must be consistent with the one of UO$_2$ to describe higher order systems such as (U, Pu, Zr, ...)O$_{2\pm x}$ solid solution. UO$_{2\pm x}$ was described by using the compound energy formalism with ionic species: (U^{3+}, U^{4+}, U^{6+})$_1$(O^{2-}, Va)$_2$(O^{2-}, Va)$_1$ [10]. The compound energy model has been successfully used by Grundy et al. [73] to describe both defect chemistry and thermochemical properties of LaMnO$_{3\pm d}$ perovskite and by Zinkevich et al. [9] to model the thermodynamic properties of the oxide phases for the cerium–oxygen system. Grundy et al. have shown that the compound energy formalism is more appropriate than the associate model to describe such systems.

In case of PuO_{2-x}, the reported major defects are oxygen vacancies associated to the formation of Pu^{3+} cations. In Kröger–Vink notation the reduction reaction associated to the point defect formation is given by

$$1/2 O_O^\times + Pu_{Pu}^\times \leftrightarrow 1/2 V_O^{\cdot\cdot} + Pu'_{Pu} + 1/4 O_2(g) \tag{3}$$
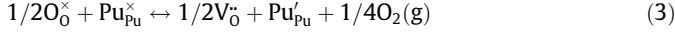
where $O_O^\times$ and $Pu_{Pu}^\times$ represent the perfect sites of the crystal, and $V_O^{\cdot\cdot}$ and Pu'_{Pu} designate, respectively, doubly positively charged oxygen vacancies and reduced plutonium ions (Pu^{3+}).

For this reaction, the equilibrium constant K_r is defined by

$$K_r = \frac{[V_O^{\cdot\cdot}]^{1/2}[Pu'_{Pu}]p_{O_2}^{1/4}}{[O_O^\times]^{1/2}[Pu_{Pu}^\times]} \tag{4}$$

For small defect concentrations, $[O_O^\times]$ and $[Pu_{Pu}^\times]$ can be considered to be equal to ~ 1.

In order to maintain charge neutrality the following relation must be hold:

$$[V_O^{\cdot\cdot}] = 2[Pu'_{Pu}] \tag{5}$$

Combining Eqs. (4) and (5), the following proportionality between defect concentration and oxygen partial pressure is obtained:

$$\log[Pu'_{Pu}] \propto \log p_{O_2}^{-1/6} \quad \text{and} \quad \log[V_O^{\cdot\cdot}] \propto \log p_{O_2}^{-1/6} \tag{6}$$

In the classical defect modelling, the equilibrium constant K_r is adjusted to fit the experimental data on oxygen chemical potential data versus temperature and stoichiometry of the oxide, which are related to the concentration of defect.

The corresponding sublattice model to describe the non stoichiometric plutonium dioxide is

$$(Pu^{4+}, Pu^{3+})_1 (O^{2-}, Va)_2 \tag{7}$$

The first and second sublattices correspond to the crystallographic sites in the fluorite structure, of respectively plutonium and oxygen atoms. Oxygen vacancies are added in the oxygen site that are associated with Pu^{3+} formation.

The defect reaction in the sublattice notation is:

$$(Pu^{4+})_1(O^{2-})_2 \rightarrow (Pu^{3+})_1(O_{3/4}^{2-}, Va_{1/4})_2 + 1/4 O_2(g) \tag{8}$$
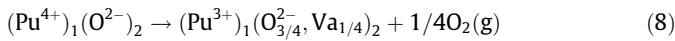
This reaction is equivalent to Eq. (3) when written in Kröger–Vink notation.

Stan et al. [7] have recently reported a thermochemical model to describe PuO_{2-x} in which more complex defects are considered: singly positively charged oxygen vacancies ($V_O^{\cdot}$), doubly positively charged oxygen vacancies ($V_O^{\cdot\cdot}$), singly positively charged metal–oxygen vacancy pairs ($(PuV_O)^{\cdot}$), neutral charged metal–oxygen vacancy pairs ($(PuV_O)^\times$) and reduced plutonium ions (Pu^{3+} ions). In the present work, we will not take into account such complex defects. The sublattice model described by Eq. (7) will be used.

The Gibbs energy associated to the sublattice model (Pu^{4+}, Pu^{3+})$_1$(O^{2-}, Va)$_2$ using the compound energy formalism [3] is given by

$$\begin{aligned}
G^\varphi - \sum_i n_i^\varphi {}^\circ H_i^{SER}(298.15\ K) &= y_{Pu^{4+}} y_{O^{2-}} {}^\circ G_{(Pu^{4+})_1(O^{2-})_2} \\
&+ y_{Pu^{4+}} y_{Va} {}^\circ G_{(Pu^{4+})_1(Va)_2} + y_{Pu^{3+}} y_{Va} {}^\circ G_{(Pu^{3+})_1(Va)_2} \\
&+ y_{Pu^{3+}} y_{O^{2-}} {}^\circ G_{(Pu^{3+})_1(O^{2-})_2} + RT(y_{Pu^{3+}} \ln y_{Pu^{3+}} + y_{Pu^{4+}} \ln y_{Pu^{4+}}) \\
&+ 2RT(y_{O^{2-}} \ln y_{O^{2-}} + y_{Va} \ln y_{Va}) + y_{Pu^{3+}} y_{Pu^{4+}} \\
&\times \Big[L^0_{(Pu^{3+}, Pu^{4+})_1(O^{2-})_2} + (y_{Pu^{3+}} - y_{Pu^{4+}}) L^1_{(Pu^{3+}, Pu^{4+})_1(O^{2-})_2} + L^0_{(Pu^{3+}, Pu^{4+})_1(Va)_2} \\
&+ (y_{Pu^{3+}} - y_{Pu^{4+}}) L^1_{(Pu^{3+}, Pu^{4+})_1(Va)_2} \Big]
\end{aligned} \tag{9}$$

where

- y_i represents the fraction of the species 'i' in the sublattice
- ${}^\circ G_{(i)_1(j)_2}$ are the Gibbs energies of the different compounds formed by considering the species 'i' in the first sublattice and the species 'j' in the second sublattice
- L^i are interaction parameters which can have a linear dependence in temperature.

The model is schematically represented in Fig. 2. The Gibbs energy of plutonia is given as a mixture of the four end members: neutral $(Pu^{4+})(O^{2-})_2$, $(Pu^{4+})(Va)_2$ with a net charge of +4, $(Pu^{3+})(Va)_2$ with a net charge of +3 and $(Pu^{3+})(O^{2-})_2$ with a net charge of −1. Three of these four end members corresponding to the four corners in Fig. 2 are hypothetical and have no physical meaning by themselves, only in electrically neutral combinations. The Gibbs energy contains also a configurational entropy term for the mixing of Pu^{4+} and Pu^{3+} cations in the first sublattice and O^{2-} anions and oxygen vacancies, 'Va', in the second sublattice. Plutonia can only exist along the neutral line shown in Fig. 2. One endpoint of the neutral line corresponds to the stoichiometric plutonia PuO_2. The other endpoint corresponds to the completely reduced plutonia $PuO_{1.5}$.

The Gibbs energy of these two compounds is given by

$${}^\circ G_{PuO_2} = {}^\circ G_{(Pu^{4+})_1(O^{2-})_2} \tag{10}$$

$${}^\circ G_{PuO_{1.5}} = \frac{3}{4} {}^\circ G_{(Pu^{3+})_1(O^{2-})_2} + \frac{1}{4} {}^\circ G_{(Pu^{3+})_1(Va)_2} + 2RT\left(\frac{1}{4}\ln\frac{1}{4} + \frac{3}{4}\ln\frac{3}{4}\right) \tag{11}$$

By fixing the following relations between the parameters:

$${}^\circ G_{(Pu^{4+})_1(Va)_2} = {}^\circ G_{(Pu^{4+})_1(O^{2-})_2} - 2{}^\circ G_O \tag{12}$$

$${}^\circ G_{(Pu^{3+})_1(Va)_2} = {}^\circ G_{(Pu^{3+})_1(O^{2-})_2} - 2{}^\circ G_O \tag{13}$$

where ${}^\circ G_O$ is the Gibbs energy of 1/2 O_2 gas, the four end members are obtained:

$${}^\circ G_{(Pu^{4+})_1(O^{2-})_2} = {}^\circ G_{PuO_2} \tag{14}$$

$${}^\circ G_{(Pu^{4+})_1(Va)_2} = {}^\circ G_{PuO_2} - 2{}^\circ G_O \tag{15}$$

$${}^\circ G_{(Pu^{3+})_1(Va)_2} = {}^\circ G_{PuO_{1.5}} - \frac{3}{2} {}^\circ G_O - 2RT\left(\frac{1}{4}\ln\frac{1}{4} + \frac{3}{4}\ln\frac{3}{4}\right) \tag{16}$$

$${}^\circ G_{(Pu^{3+})_1(O^{2-})_2} = {}^\circ G_{PuO_{1.5}} + \frac{1}{2} {}^\circ G_O - 2RT\left(\frac{1}{4}\ln\frac{1}{4} + \frac{3}{4}\ln\frac{3}{4}\right) \tag{17}$$

The parameters that have to be assessed in the model are ${}^\circ G_{PuO_2}$, ${}^\circ G_{PuO_{1.5}}$ and the interaction parameters L^i. Thermodynamic data for pure PuO_2 from the SGTE substance database are taken as initial parameters [42,44]. The enthalpy and entropy terms have been optimized.
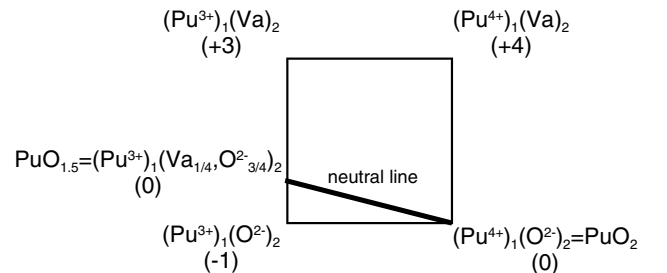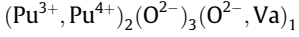

$(Pu^{3+})_1(Va)_2$ (+3) $(Pu^{4+})_1(Va)_2$ (+4)

$PuO_{1.5} = (Pu^{3+})_1(Va_{1/4}, O^{2-}_{3/4})_2$ (0) neutral line

$(Pu^{3+})_1(O^{2-})_2$ (-1) $(Pu^{4+})_1(O^{2-})_2 = PuO_2$ (0)

Fig. 2. Schematic representation of the sublattice model (Pu^{3+}, Pu^{4+})1(O^{2-}, Va)$_2$ to describe plutonia PuO_{2-x}.

3.4. PuO$_{1.61}$ bcc phase

The sublattice model to describe the cubic Ce$_3$O$_{5\pm x}$ in [9] is used:

$$(Pu^{3+}, Pu^{4+})_2 (O^{2-})_3 (O^{2-}, Va)_1$$

The variable oxygen content in the phase is compensated by changing the oxidation state of plutonium from +3 to +4. Two neutral compositions are obtained for the end members:

– $(Pu^{4+})_2(O^{2-})_3(O^{2-})_1$ with a composition PuO$_2$ which corresponds to a metastable cubic PuO$_2$ phase with respect to the fluorite form;
– $(Pu^{3+})_2(O^{2-})_3(Va)_1$ with a composition Pu$_2$O$_3$ which corresponds to the metastable cubic Pu$_2$O$_3$ phase with respect to the hexagonal form.

The Gibbs energy of the phase is given by

$$
\begin{aligned}
G^{\varphi} - \sum_i n_i^{\varphi \circ} H_i^{SER} \ (298.15 \ K) &= y_{Pu^{4+}} y_{O^{2-}} {}^{\circ}G_{(Pu^{4+})_2(O^{2-})_3(O^{2-})_1} \\
&+ y_{Pu^{4+}} y_{Va} {}^{\circ}G_{(Pu^{4+})_2(O^{2-})_3(Va)_1} + y_{Pu^{3+}} y_{Va} {}^{\circ}G_{(Pu^{3+})_2(O^{2-})_3(Va)_1} \\
&+ y_{Pu^{3+}} y_{O^{2-}} {}^{\circ}G_{(Pu^{3+})_2(O^{2-})_3(O^{2-})_1} + 2RT(y_{Pu^{3+}} \ln y_{Pu^{3+}} + y_{Pu^{4+}} \ln y_{Pu^{4+}}) \\
&+ RT(y_{O^{2-}} \ln y_{O^{2-}} + y_{Va} \ln y_{Va}) + y_{Pu^{3+}} y_{Pu^{4+}} \Big[L^0_{(Pu^{3+}, Pu^{4+})_2(O^{2-})_3(O^{2-})_1} \\
&+ (y_{Pu^{3+}} - y_{Pu^{4+}}) L^1_{(Pu^{3+}, Pu^{4+})_2(O^{2-})_3(O^{2-})_1} + L^0_{(Pu^{3+}, Pu^{4+})_2(O^{2-})_3(Va)_1} \\
&+ (y_{Pu^{3+}} - y_{Pu^{4+}}) L^1_{(Pu^{3+}, Pu^{4+})_2(O^{2-})_3(Va)_1} \Big]
\end{aligned}
\tag{18}
$$

The Gibbs energy parameters for PuO$_{1.61}$ are expressed from the parameters of fcc PuO$_{2-x}$ phase by

$$\lfloor {}^{\circ}G_{(Pu^{3+})_2(O^{2-})_3(O^{2-})_1} \rfloor_{PuO_{1.61}} = 2 \left[{}^{\circ}G_{PuO_{1.5}} \right]_{PuO_2}^{fcc} + {}^{\circ}G_O + V1 + V10T \tag{19}$$

$$\lfloor {}^{\circ}G_{(Pu^{3+})_2(O^{2-})_3(Va)_1} \rfloor_{PuO_{1.61}} = 2 \left[{}^{\circ}G_{PuO_{1.5}} \right]_{PuO_2}^{fcc} + V1 + V10T \tag{20}$$

$$\lfloor {}^{\circ}G_{(Pu^{4+})_2(O^{2-})_3(Va)_1} \rfloor_{PuO_{1.61}} = 2 \left[{}^{\circ}G_{PuO_2} \right]_{PuO_2}^{fcc} + V2 + V20T \tag{21}$$

$$\lfloor {}^{\circ}G_{(Pu^{4+})_2(O^{2-})_3(O^{2-})_1} \rfloor_{PuO_{1.61}} = 2 \left[{}^{\circ}G_{PuO_2} \right]_{PuO_2}^{fcc} + V2 + V20T \tag{22}$$

where V1, V10, V2 and V2O are optimized variables. In addition, the interaction parameters $L^0_{(Pu^{3+}, Pu^{4+})_2(O^{2-})_3(O^{2-})_1} = L^0_{(Pu^{3+}, Pu^{4+})_2(O^{2-})_3(Va)_1} = V3 + V30T$ are optimized.

3.5. Liquid phase

The ionic two-sublattice model is used to describe the liquid phase [74]:

$$(Pu^{3+})_P (O^{2-}, Va^{Q-}, PuO_2, O)_Q$$
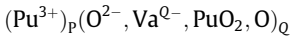
In this model, the first sublattice contains the Pu^{3+} cation; the second one contains the O^{2-} anions, some charged vacancies (Va^{Q-}) and the neutral species PuO$_2$ and O.

P and Q are equal to the average charge of the opposite sublattice:

$$P = Q y_{Va^{Q-}} + 2 y_{O^{2-}} \quad \text{and} \quad Q = 3 \tag{23}$$

The induced charge of the vacancies corresponds to Q = 3. P varies via the site fractions of the species with the composition in the second sublattice in order to maintain the liquid phase electrically neutral. The Gibbs energy of the liquid phase is given by the following expression:

$$
\begin{aligned}
G^{liquid} &= y_{O^{2-}} {}^{\circ}G_{(Pu^{3+})_2(O^{2-})_3} + y_{Va^{Q-}} {}^{\circ}G_{Pu} + y_{PuO_2} {}^{\circ}G_{PuO_2} + y_O {}^{\circ}G_O \\
&+ QRT(y_{O^{2-}} \ln y_{O^{2-}} + y_{Va^{Q-}} \ln y_{Va^{Q-}} + y_{PuO_2} \ln y_{PuO_2} \\
&+ y_O \ln y_O) + y_{O^{2-}} y_{Va^{Q-}} [L^0 + (y_{O^{2-}} - y_{Va^{Q-}}) L^1] \\
&+ y_{O^{2-}} y_{PuO_2} (L^0 + (y_{O^{2-}} - y_{PuO_2}) L^1]
\end{aligned}
\tag{24}
$$

${}^{\circ}G_{(Pu^{3+})_2(O^{2-})_3}$, ${}^{\circ}G_{Pu}$, ${}^{\circ}G_{PuO_2}$ and ${}^{\circ}G_O$ are the reference terms corresponding to the Gibbs energy of respectively sesquioxide Pu$_2$O$_3$, pure plutonium, dioxide PuO$_2$ and pure oxygen. The Gibbs energy of the liquid phase contains a configurational entropy term related to mixing of the species in the second sublattice. Excess terms related to mixing of Pu and Pu$_2$O$_3$ (i.e. between the constituents O^{2-} and Va^{Q-}) are assessed to represent the miscibility gap in the liquid state of the phase diagram. Interaction parameters between Pu$_2$O$_3$ and PuO$_2$ (i.e. the constituents O^{2-} and PuO$_2$) are added to fit the liquidus data. The melting enthalpy and entropy for the neutral combinations of the liquid constituents are taken from the SGTE substance database [44,42].

3.6. Gas phase

The gas phase is described by an ideal mixture of (Pu, PuO, PuO$_2$, O, O$_2$, O$_3$) gaseous species. The Gibbs energy is expressed by

$$G^{\varphi} = \sum_i y_i {}^{\circ}G_i^{\varphi} + RT \sum_i y_i \ln y_i + RT \ln P/P_0 \tag{25}$$

where y_i is the fraction of the species 'i' in the gas phase. ${}^{\circ}G_i^{\varphi}$ represents the standard Gibbs energy of the gaseous species 'i'. P_0 is the standard pressure. The functions are extracted from the SGTE substance database [44,42].

4. Results and discussion

The calculated temperatures and phase compositions for all the invariant reactions and the associated thermodynamic assessed parameters are listed in respectively Tables 3 and 4.

The calculated phase diagram is presented in Fig. 3. A comparison with the experimental data is given in Figs. 4 and 5. In the Pu–Pu$_2$O$_3$ part, the present assessment reproduces the existence of the miscibility gap in the liquid state but no real assessment can be done due to lack of experimental data in this part of the phase diagram, especially data on the oxygen solubility limit in liquid plutonium. The most investigated region is the Pu$_2$O$_3$–PuO$_2$ part. Considering the few available experimental data in this region, the main features of the phase diagram are well reproduced: the wide composition range of PuO$_{2-x}$ at high temperature, the composition range and the congruent decomposition of the PuO$_{1.61}$ phase and the narrow miscibility gap in the PuO$_{2-x}$ phase. The present thermodynamic model leads to a good representation of the diagram proposed by Wriedt [14] based on the investigations of Sari et al. [21] and Besmann [25].

The calculated enthalpy increment for PuO$_2$ versus temperature is presented in Fig. 6. These calculations are based on the properties of PuO$_2$ reported in the SGTE substance database [42,44]. The rapid increase in C_p above 2370 K is not reproduced. As mentioned in the previous Section 2.5.1, this phenomenon would require a confirmation by performing new measurements.

The calculated thermodynamic properties of the different plutonium oxides at 298.15 K are compared to data of the literature in Table 5. A good agreement is obtained. A deviation of 4 kJ/mol is obtained for the calculated enthalpy of formation for PuO$_2$ with respect to the value recommended value by Lemire et al. [43]. But considering the resulting relative error of 0.4%, this deviation is not high (see Tables 4 and 5).

The partial enthalpy of O$_2$ is calculated at 1373 K and compared to the experimental data of Chereau et al. [46] and Dean et al. [24] as well as the values derived from oxygen chemical measurements of Markin et al. [28] and Woodley [55] in Fig. 7. The discrepancies between the experimental data are the same than those reported for the oxygen chemical potential data. A good agreement is obtained between our calculations and the experimental data of Dean

Table 3
Invariant reactions in the Pu–O system

Data	T (K)	Compositions of the phases	Reference
L = G	**4097**	**62.3 (L,G)**	Present work
L = G	**3410**	**32.5 (L,G)**	Present work
L = G + PuO$_{2-x}$	**2640**	**66.5 (PuO_{2-x}), 66.8 (L)**	Present work
L2 = L1 + Pu$_2$O$_3$	2098 ± 40	10 (L1), 50 (L2)	Martin [13]
	2098	8 (L1), 50 (L2)	Wriedt [14]
	2122	**10 ($L1$), 49.7 ($L2$)**	Present work
Pu$_2$O$_3$ = L	2358 ± 25		Chikalla [12]
	2348 ± 5		Riley [29]
	2353		Wriedt [14]
	2330		Present work
L = Pu$_2$O$_3$ + PuO$_2$	2273	60.5 (L)	Wriedt [14]
	2306	**60.5 (L), 61.5 (PuO_{2-x})**	Present work
PuO$_2$ = L	2673		Russel [30]
	2553 ± 30		Chikalla [12]
	2718		Aitken [40]
	2673 ± 20		Riley [29]
	2698		Wriedt [14]
	2660	**66.2 (PuO_2, L)**	Present work
PuO$_{2-x}$ = PuO$_{1.61}$	~1450		Besmann [25]
	~1450		Wriedt [14]
	1445	**62.4 (PuO_{2-x}, $PuO_{1.61}$)**	Present work
PuO$_{2-x}$ = Pu$_2$O$_3$ + PuO$_{1.61}$	~1353	61.5 (PuO$_2$), 61.8 (PuO$_{1.61}$)	Besmann [25]
	~1353	61.6 (PuO$_2$), 62 (PuO$_{1.61}$)	Wriedt [14]
	1422	**61.9 (PuO_{2-x}, $PuO_{1.61}$)**	Present work
PuO$_{1.52}$ = Pu$_2$O$_3$ + PuO$_{1.61}$	573–623		Boivineau [20]
	623	61.7 ($PuO_{1.61}$)	Gardner [23]
	743–753	61.9 (PuO$_{1.61}$)	Sari [21]
	723	61.9 (PuO$_{1.61}$)	Wriedt [14]
	711	**61.7 ($PuO_{1.61}$)**	Present work
PuO$_{1.61}$ = PuO$_{1.52}$ + PuO$_2$	573	63 (PuO$_{1.61}$), 66.4 (PuO$_{2-x}$)	Chikalla [12]
	573	61.7 (PuO$_{1.61}$)	Gardner [23]
	573	61.7 (PuO$_{1.61}$), 66.6 (PuO$_{2-x}$)	Boivineau [20]
	608	63 (PuO$_{1.61}$), 66.5 (PuO$_{2-x}$)	Sari [21]
	608	62 (PuO$_{1.61}$), 66.6 (PuO$_{2-x}$)	Wriedt [14]
	576	**61.8 ($PuO_{1.61}$), 66.62 (PuO_{2-x})**	Present work
PuO$_2$(2) = PuO$_{1.61}$ + PuO$_2$(1)	943	63.2 (PuO$_{1.61}$), 66 (PuO$_2$(1))	Boivineau [20]
	903	62.8 (PuO$_{1.61}$), 62.9 (PuO$_2$(2)), 66.5 (PuO$_2$(1))	Sari [21]
	903	62.8 (PuO$_{1.61}$), 62.9 (PuO$_2$(2)), 66.5 (PuO$_2$(1))	Wriedt [14]
	987	**63.2 ($PuO_{1.61}$), 63.8 (PuO_2 (2)), 66.2 (PuO_2 (1))**	Present work
L = ε-Pu + Pu$_2$O$_3$	**912**		Present work
ε-Pu = δ′-Pu	**756**		Present work
δ′-Pu = δ-Pu	**736**		Present work
δ-Pu = γ-Pu	**593**		Present work
γ-Pu = β-Pu	**488**		Present work
β-Pu = α-Pu	**398**		Present work

et al. [24]. The highest values of Chereau et al. [46] that are consistent with those of Woodley [55] could not be well reproduced even when the data of Chereau et al. were selected for the optimization. The calculated variation of oxygen partial enthalpy with composition is consistent with the phase diagrams proposed by Sari et al. [21] and Besmann [25] concerning the existence of a large composition range for PuO$_{1.61}$ phase and a narrow two-phase domain [PuO$_{1.61+x}$ + PuO$_{2-x}$] [21]. The existence of this narrow two-phase domain [PuO$_{1.61}$ + PuO$_{2-x}$] proposed by Chereau et al. [46] and the corresponding calculated oxygen partial enthalpy are very well reproduced. Experimental data on the phase equilibria in this temperature range are missing to fix definitively the temperature of decomposition of the PuO$_{1.61}$ phase.

The O$_2$ partial Gibbs energy has been calculated for all the two-phase equilibria in Fig. 8 where experimental data are reported. A good agreement is obtained with the data of Besmann [25] and Tetenbaum [60]. The calculated data are significantly lower than the measurements by Markin et al. [45].

The results of the calculations in the PuO$_{2-x}$ composition range are presented in Fig. 9 as $\mu(O_2)$ versus log(x) for fixed temperatures ranging from 1100 K to 2100 K and in Fig. 10 as $\mu(O_2)$ versus temperature for fixed O/Pu ratios ranging from 1.7 to 1.995. With both types of representations, as mentioned in the previous section, it can be noted that below 1500 K, the experimental data are scattered. The differences in the experimental conditions (temperature and O/Pu ratio) cannot explain such large discrepancies. An overall good agreement is obtained between the calculations and the selected data of Swansson et al. [56], Woodley [55], and Tetenbaum [60]. The highest discrepancy with the experimental data is obtained with the data of Atlas et al. [58] Kent et al. [59] and Markin et al. [28] as for the two-phase domains (see Fig. 8).

Table 4
Assessed thermodynamic parameters for the Pu–O system, referred to stable element reference H^{SER} ($T = 298.15$ K, $P = 1$ bar) (present work) – values in J, K, mol, Pa

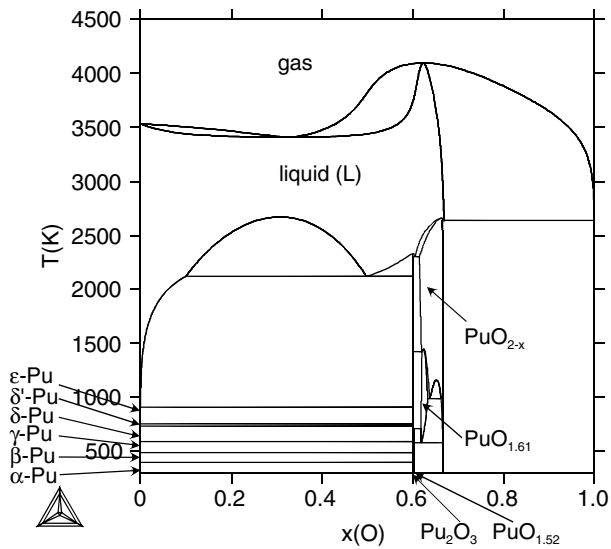| Phase	Gibbs energy (J/mol)		Reference
Liquid $(Pu^{3+})_P(O^{2-},Va^{Q-},PuO_2,O)_Q$	$^\circ G_{(Pu^{3+})_2(O^{2-})_3} - 3^\circ H_O^{SER} - 2^\circ H_{Pu}^{SER} = G_{Pu_2O_3} + 113\,000 - 47.921967\,T$		[44]
	$^\circ G_{(Pu^{+3})_1(Va^{-1})_3} - ^\circ H_{Pu}^{SER} = G_{Pu}^{liq}$		[72]
	$^\circ G_{PuO_2} - 2^\circ H_O^{SER} - ^\circ H_{Pu}^{SER} = G_{PuO_2} + 67\,000 - 25.1595944\,T$		[44]
	$^\circ G_O - ^\circ H_O^{SER} = G_O^{liq}$		[72]
	$L^0_{(Pu^{3+})_P(O^{2-},Va)_Q} = +123\,284$		This work
	$L^1_{(Pu^{3+})_P(O^{2-},Va)_Q} = -27\,016$		This work
	$L^0_{(Pu^{3+})_P(O^{2-},PuO_2)_Q} = +65\,272 - 2.847\,T$		This work
	$L^1_{(Pu^{3+})_P(O^{2-},PuO_2)_Q} = -10\,009$		This work
PuO_{2-x} $(Pu^{4+},Pu^{4+})_1(O^{2-},Va)_2$	$^\circ G_{(Pu^{4+})_1(O^{2-})_2} - 2^\circ H_O^{SER} - ^\circ H_{Pu}^{SER} = G_{PuO_2}$		This work C_p from [44]
	$^\circ G_{(Pu^{3+})_1(O^{2-})_2} - 2^\circ H_O^{SER} - ^\circ H_{Pu}^{SER} = G_{(Pu^{3+})_1(Va)_2} + 2G_O$		This work
	$^\circ G_{(Pu^{3+})_1(Va)_2} - ^\circ H_{Pu}^{SER} = G_{PuO_{1.5}} - 1.5G_O + 1.12467RT$		This work
	$^\circ G_{(Pu^{4+})_1(Va)_2} - ^\circ H_{Pu}^{SER} = G_{PuO_2} - 2G_O + 4540.3$		This work
	$L^0_{(Pu^{3+},Pu^{4+})_1(O^{2-})_2} = L^0_{(Pu^{3+},Pu^{4+})_1(Va)_2} = +8734.9 + 0.403\,T$		This work
	$L^1_{(Pu^{3+},Pu^{4+})_1(O^{2-})_2} = L^1_{(Pu^{3+},Pu^{4+})_1(Va)_2} = -19823.2 + 2.289\,T$		This work
$PuO_{1.61}$ $(Pu^{3+},Pu^{4+})_2(O^{2-})_3(O^{2-},Va)_1$	$^\circ G_{(Pu^{4+})_2(O^{2-})_3(O^{2-})_1} - 4^\circ H_O^{SER} - 2^\circ H_{Pu}^{SER} = 2G_{PuO_2} + 6701.94 + 12.716\,T$		This work
	$^\circ G_{(Pu^{3+})_2(O^{2-})_3(O^{2-})_1} - 4^\circ H_O^{SER} - 2^\circ H_{Pu}^{SER} = 2G_{PuO_{1.5}} + G_O - 12888.5 + 9.813\,T$		This work
	$^\circ G_{(Pu^{3+})_2(O^{2-})_3(Va)_1} - 3^\circ H_O^{SER} - 2^\circ H_{Pu}^{SER} = 2G_{PuO_{1.5}} - 12888.5 + 9.813\,T$		This work
	$^\circ G_{(Pu^{4+})_2(O^{2-})_3(Va)_1} - 3^\circ H_O^{SER} - 2^\circ H_{Pu}^{SER} = 2G_{PuO_2} - G_O + 6701.94 + 12.716\,T$		This work
	$L^0_{(Pu^{3+},Pu^{4+})_2(O^{2-})_3(O^{2-})_1} = L^0_{(Pu^{3+},Pu^{4+})_2(O^{2-})_3(Va)_1} = 27212.2 - 28.187\,T$		This work
$PuO_{1.52}$	$^\circ G_{PuO_{1.52}} - 1.52^\circ H_O^{SER} - ^\circ H_{Pu}^{SER} = -859\,900 + 345.87376\,T - 62.351\,T\ln(T) - 0.007085\,T^2 - 1.6625 \cdot 10^{-11}\,T^3 + 396\,830\,T^{-1}$		This work +C_p from [8]
Pu_2O_3	$^\circ G_{Pu_2O_3} - 3^\circ H_O^{SER} - 2^\circ H_{Pu}^{SER} = G_{Pu_2O_3}$		This work +C_p from [44]
Gas $(Pu, PuO,PuO_2,O,O_2,O_3)$	$^\circ G_{Pu}^{gas} = G_{Pu}^G + RT\ln(10^{-5}P)$		[42,44]
	$^\circ G_{PuO}^{gas} = G_{PuO}^G + RT\ln(10^{-5}P)$		
	$^\circ G_{PuO_2}^{gas} = G_{PuO_2}^G + RT\ln(10^{-5}P)$		
Functions	$G_O = ^\circ G_{1/2O_{2}(g)}$		[72]
	$G_{PuO_2} = -1091829.07 + 505.6690794\,T - 83.31922\,T\text{Ln}(T) - 0.00584178\,T^2 - 2.29241167 \cdot 10^{-11}\,T^3 + 913\,506\,T^{(-1)}$	$(298.15 < T < 2663$ K$)$	This work +C_p from [44]
	$\quad -1176688.66 + 898.5073648\,T - 131\,T\text{Ln}(T) + 7.77918 \cdot 10^{-17}\,T^2 - 2.17490333 \cdot 10^{-21}\,T^3 + 3.521756 \cdot 10^{-7}\,T^{(-1)}$	$(2663 < T < 6000$ K$)$	
	$G_{Pu_2O_3} = -1655050 - 295.6871238\,T + 38.63916\,T\text{Ln}(T) - 0.2750007\,T^2 + 7.79827167 \cdot 10^{-5}\,T^3 - 1479357.5\,T^{(-1)}$	$(298.15 < T < 400$ K$)$	This work +C_p from [44]
	$\quad -1699102.3 + 676.8695092\,T - 122.9535\,T\text{Ln}(T) - 0.014273645\,T^2 - 3.27260333 \cdot 10^{-11}\,T^3 + 750\,595\,T^{(-1)}$	$(400 < T < 2358$ K$)$	
	$\quad -1800776.63 + 1284.775875\,T - 200\,T\text{Ln}(T) + 4.1974775 \cdot 10^{-16}\,T^2 - 1.3924665 \cdot 10^{-20}\,T^3 + 2.016497 \cdot 10^{-6}\,T^{(-1)}$	$(2358 < T < 5500$ K$)$	
	$G_{PuO_{1.5}} = 1/2G_{Pu_2O_3} + 5045.18$		This work
	$G_{Pu}^G = +342384.474 - 43.117293\,T - 20.30369\,T\ln(T) + .004361944\,T^2 - 4.196665 \times 10^{-6}\,T^3 - 40656.38\,T^{(-1)}$	$(298 < T < 500$ K$)$	[42,44]
	$\quad +348176.952 - 149.678011\,T - 3.216571\,T\ln(T) - .017818755\,T^2 + 1.14424717 \times 10^{-6}\,T^3 - 405372.75\,T^{(-1)}$	$(500 < T < 1000$ K$)$	
	$\quad +358979.665 - 233.202672\,T + 8.216251\,T\ln(T) - .0225557\,T^2 + 1.4126845 \times 10^{-6}\,T^3 - 2190253.5\,T^{(-1)}$	$(1000 < T < 2000$ K$)$	
	$\quad +251181.98 + 397.043295\,T - 75.00843\,T\ln(T) + .00595168\,T^2 - 4.15198333 \times 10^{-7}\,T^3 + 23\,940\,665\,T^{(-1)}$	$(2000 < T < 3200$ K$)$	
	$\quad +538268.521 - 759.796803\,T + 69.56718\,T\ln(T) - .026257465\,T^2 + 9.247795 \times 10^{-7}\,T^3 - 82\,378\,450\,T^{(-1)}$	$(3200 < T < 4700$ K$)$	
	$\quad -455390.692 + 1948.02049\,T - 251.164\,T\ln(T) + .01987852\,T^2 - 3.22796833 \times 10^{-7}\,T^3 + 4.9645555 \times 10^8\,T^{(-1)}$	$(4700 < T < 7600$ K$)$	
	$\quad +430311.346 + 352.921981\,T - 72.15296\,T\ln(T) + .0037501715\,T^2 - 4.95895 \times 10^{-8}\,T^3 - 3.278732 \times 10^8\,T^{(-1)}$	$(7600 < T < 10\,000$ K$)$	
	$G_{PuO}^G = -81162.9184 + 84.1696968\,T - 47.48987\,T\ln(T) - .015822525\,T^2 + 8.07580833 \times 10^{-6}\,T^3 + 611\,710\,T^{(-1)}$	$(298 < T < 500$ K$)$	[42,44]
	$\quad -91376.0436 + 303.962443\,T - 83.63347\,T\ln(T) + .03789824\,T^2 - 6.28436167 \times 10^{-6}\,T^3 + 1107078.5\,T^{(-1)}$	$(500 < T < 900$ K$)$	
	$\quad -47108.7524 - 191.469738\,T - 10.96509\,T\ln(T) - .015103325\,T^2 + 9.614135 \times 10^{-7}\,T^3 - 3947626\,T^{(-1)}$	$(900 < T < 2100$ K$)$	
	$\quad -115058.704 + 228.613287\,T - 66.82868\,T\ln(T) + .004912038\,T^2 - 3.63050333 \times 10^{-7}\,T^3 + 11\,143\,440\,T^{(-1)}$	$(2100 < T < 3800$ K$)$	
	$\quad +121688.998 - 675.810691\,T + 45.15148\,T\ln(T) - .018010055\,T^2 + 4.99610333 \times 10^{-7}\,T^3 - 79\,194\,500\,T^{(-1)}$	$(3800 < T < 5900$ K$)$	
	$\quad -680904.18 + 1217.5518\,T - 174.7726\,T\ln(T) + .008701535\,T^2 - 1.0718605 \times 10^{-7}\,T^3 + 4.683995 \times 10^8\,T^{(-1)}$	$(5900 < T < 10\,000$ K$)$	
	$G_{PuO_2}^G = -425666.047 - 6.46777282\,T - 38.18547\,T\ln(T) - .02954761\,T^2 + 4.77444167 \times 10^{-6}\,T^3 - 70282.85\,T^{(-1)}$	$(298 < T < 800$ K$)$	[42,44]
	$\quad -444201.953 + 230.692788\,T - 73.77683\,T\ln(T) + 6.714505 \times 10^{-4}\,T^2 - 1.33627967 \times 10^{-8}\,T^3 + 1729839\,T^{(-1)}$	$(800 < T < 6000$ K$)$	
	$\quad -453866.82 + 239.96684\,T - 74.63718\,T\ln(T) + 5.42008 \times 10^{-4}\,T^2 - 4.87475833 \times 10^{-9}\,T^3 + 12\,258\,850\,T^{(-1)}$	$(6000 < T < 10\,000$ K$)$	

Fig. 3. Calculated phase diagram of the Pu–O system in atomic fraction of oxygen (present work).

The relation between the variation of the oxygen chemical potential with composition and temperature and the phase diagram is represented in Fig. 11 where the calculated curves $\log 10(pO_2)$ versus O/Pu ratio for temperatures ranging from 1023 to 2250 K are given. The associated phase boundaries are indicated. The plateaus correspond to the two-phase regions. The present modelling of the thermodynamic data of the oxide phases Pu_2O_3, $PuO_{1.52}$, $PuO_{1.61}$ and PuO_{2-x} is consistent with the phase diagram proposed by Wriedt [14] and Besmann [25]. The extent of the present modelling to the description of ternary systems such as U–Pu–O and Pu–O–C will be interesting to validate the selection of the experimental data performed in the present work.

The vaporisation behaviour of the Pu–O system is studied by performing calculations from the present modelling of the condensed phases and using the thermodynamic data reported in [44] for the gaseous species Pu(g), PuO(g) and PuO_2(g). These thermodynamic data come from the compilation published by Glushko et al. [42]. The first calculations of vapour pressure data are performed above the two-phase [Pu_2O_3–$PuO_{1.61}$] domain. In Fig. 12, the calculated total and partial pressures of PuO(g), Pu(g) and PuO_2(g) are compared to the available experimental data of Ackermann et al. [64], Ohse et al. [27], Messier [26], Phipps et al. [63] and Battles et al. [65]. In all of these studies, the total pressure was measured with the assumption of PuO(g) as main species, later confirmed by Battles et al. [65]. Our calculations lead to identical results for the total pressure and PuO(g) partial pressures. A good agreement is found between our calculations and the experimental data for the total pressure considering PuO(g) as the major species. Such a result is consistent with the way that Glushko et al. [42] selected their data for the condensed phases and for the PuO(g) species. The calculated partial pressures of Pu(g) are not consistent with the set of independent data from Battles et al. [65]. In the contrary our results are in good agreement with the data of Ackermann et al. [64] who performed a thermodynamic analysis of the Pu–O system from their pressure measurements and using the data of Markin [45] for the oxygen potential data in PuO_{2-x} and for the thermodynamic data of Pu_2O_3 and $PuO_{1.61}$ solid phases.

To complete the present results, the vaporization of plutonia is studied. As reported in the previous section, a congruent vaporization is found for a O/Pu ratio around 1.82. The calculated and experimental congruent compositions of PuO_{2-x} versus temperature are reported in Fig. 13. Two cases are considered in our calculations. In the first case, the calculations are performed by fixing as a condition that the compositions of both gas and PuO_{2-x} phases are equal. It corresponds to the azeotropic composition representing the vaporization of plutonia in a closed system. In all the available experiments, a Knudsen cell was used to evaporate the material. Such conditions correspond to an open system that require to consider the flow of the different gaseous species and that lead to noticeable different congruent compositions, shifted to lower oxygen contents. The effusion cell is inherently more reducing than the corresponding closed system and then it is necessary to consider the effusion flow condition in the calculations to reproduce the experiments. In such a case, the agreement between the calculations and the experimental data is good. Below 2000 K, a deviation between our calculations and the experimental data is noted that lead to a composition closer to PuO_2 in our calculations.

The calculated total pressure over PuO_{2-x} versus temperature is compared with the available experimental data in Fig. 14. In the effusion experimental works, $PuO_2(g)$ is assumed to be the major
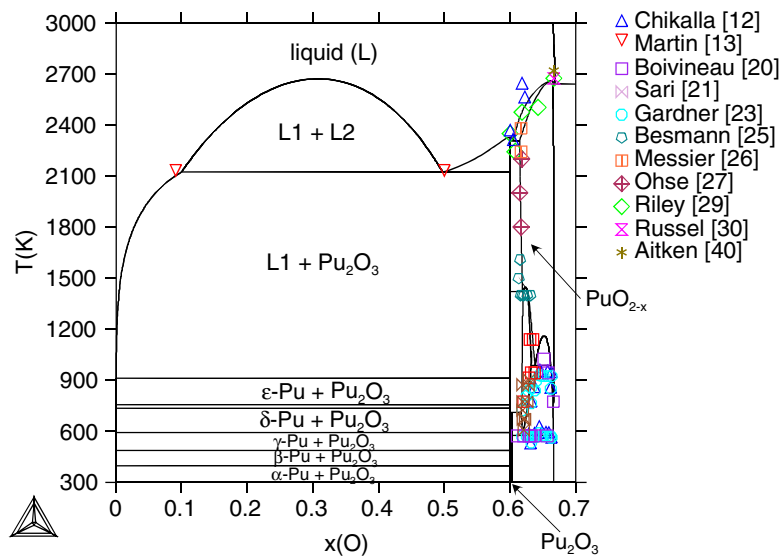

Fig. 4. Calculated phase diagram of the Pu–O system in atomic fraction of oxygen (present work) – comparison with the experimental phase boundaries.
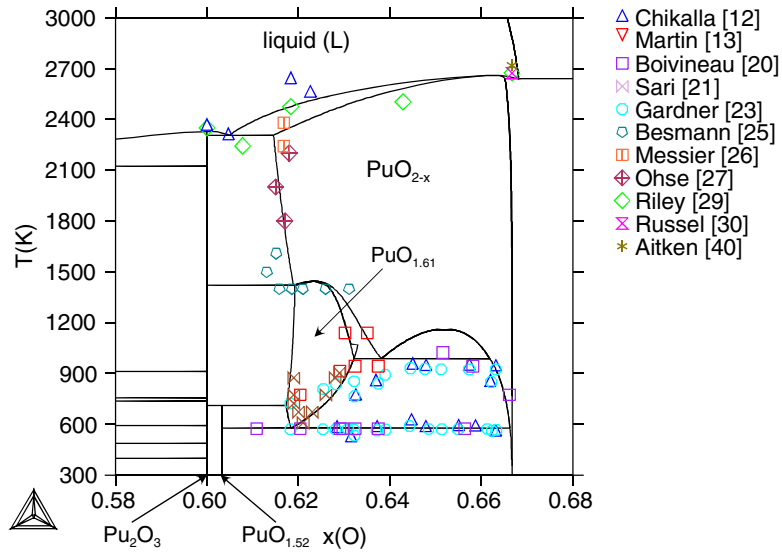
Fig. 5. Calculated phase diagram from 58 to 68 at.% O (present work) – comparison with the experimental phase boundaries.
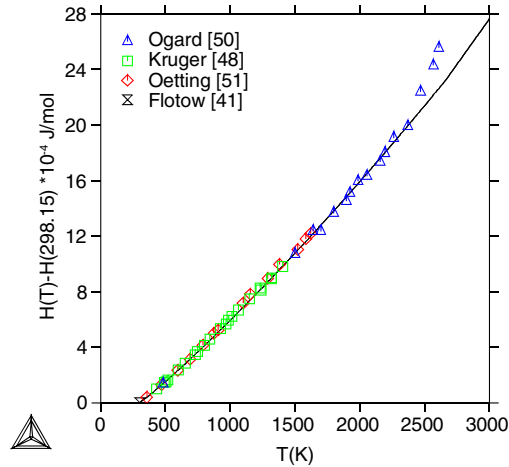

Fig. 6. Calculated enthalpy increment versus temperature for PuO$_2$ (present work, SGTE, 42) – comparison with the experimental data.

species in the gas phase to calculate the pressure. This assumption was chosen by Glushko et al. in their selection [42]. A good agreement is obtained between the experimental and calculated data.

The partial pressures of PuO(g) and PuO$_2$(g) over congruent PuO$_{2-x}$ are calculated and compared to mass spectrometric results reported by Battles et al. [65] and Kent [67] in Fig. 15. The two sets of experimental data lead to partial pressures of PuO(g) and PuO$_2$(g) which are close to each other at the congruent vaporization of PuO$_{2-x}$. But as mentioned in the previous section, the data of Kent [67] are not consistent with the measurements performed by Battles et al. [65] concerning the major species in the vapour phase: according to Kent, PuO$_2$(g) is the major species in the vapour whereas it is PuO(g) for Battles et al. [65]. This difference is difficult to explain as both authors used mass spectrometry to measure the partial pressures. The original experimental data of Kent [67] are unpublished. Our calculations which take into account the effusion flow of PuO(g) and PuO$_2$(g) species from the vapour, show a better agreement with the data of Kent [67] considering PuO$_2$(g) as the major species in the vapour. This is

Table 5
Calculated thermodynamic data for the oxide compounds (present work) – comparison with data from the literature

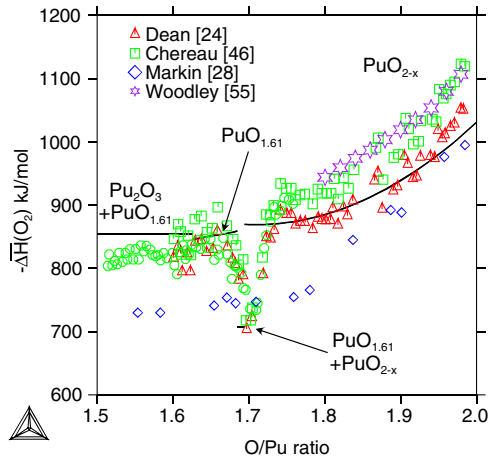| Phase	ΔH formation (298.15 K) in kJ mol^{-1}	S (298.15 K) in J mol^{-1} K^{-1}	C_p (298.15 K) in J mol^{-1} K^{-1}	Reference
Pu$_2$O$_3$	**−1656.2**	**163.4**	**117.0**	Present work
		163.2 ± 0.6	117.0 ± 0.5	Flotow [41]
	−1656			Besmann [25]
	−1654 ± 20	159.4 ± 25.1		Chereau [46]
	−1685 ± 25	142.2 ± 20.9		Markin [45]
	−1670 ± 20	163.0		Glushko et al. [42]
	−1656 ± 10	163.0 ± 0.6	117.0 ± 0.5	Lemire et al. [43]
PuO$_{1,52}$	**−838.0**	**80.4**		Present work
	−845 ± 10			Lemire et al. [43]
PuO$_{1,61}$	**−867.2**	**81.2**		Present work
	−895 ± 6	80.3 ± 10.5		Markin [45]
	−884.5 ± 16.7	87.0 ± 16.7		Chereau [46]
	−875.5 ± 10	83.0 ± 5	61.2 ± 5	Lemire et al. [43]
PuO$_2$	**−1060.3**	**66.13**	**66.25**	Present work
	−1056.0 ± 4.0			Popov [53]
	−1058.0 ± 1.6 kJ/mol			Holley [11]
	−1055.7 ± 0.72			Johnson [54]
		66.13 ± 0.3	66.24	Flotow [41]
	−1055.8 ± 0.8	66.13		Glushko et al. [42]
	−1055.8 ± 1.0	66.13 ± 0.26	66.25 ± 0.26	Lemire et al. [43]

Fig. 7. Calculated partial enthalpy of O_2 as a function of the O/Pu ratio at 1373 K (present work) – comparison with the experimental data.
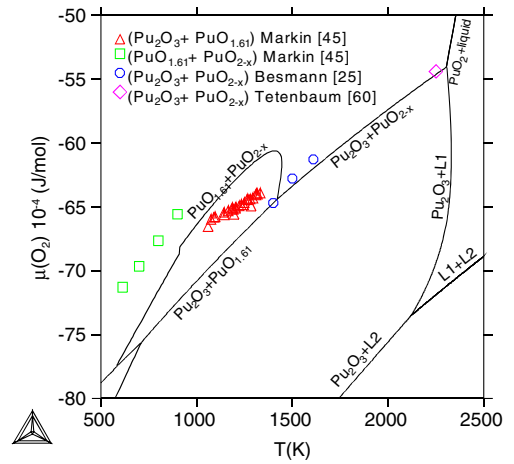

Fig. 8. Calculated $\Delta G(O_2)$ versus temperature in two-phase domains of the Pu–O system (present work) – comparison with the experimental data.
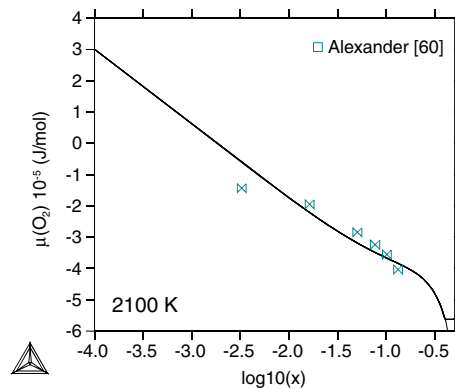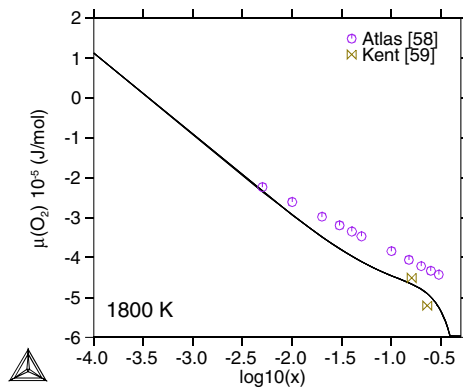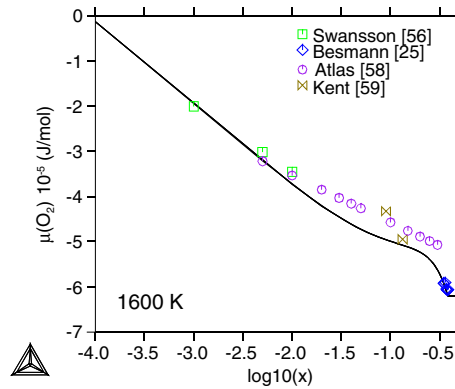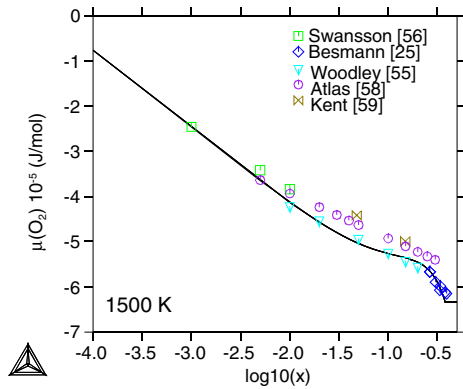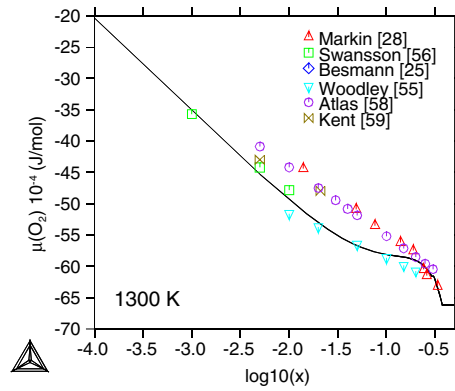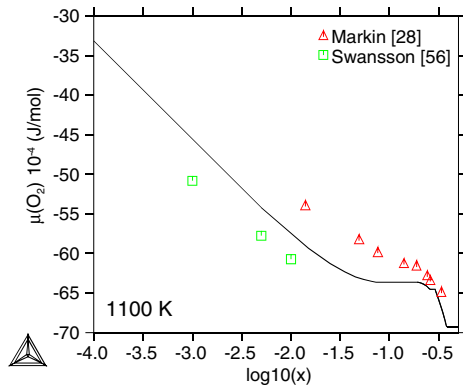

Fig. 9. Calculated $\Delta G(O_2)$ versus $\log(x)$ in PuO_{2-x} at fixed temperatures (present work) – comparison with the experimental data.
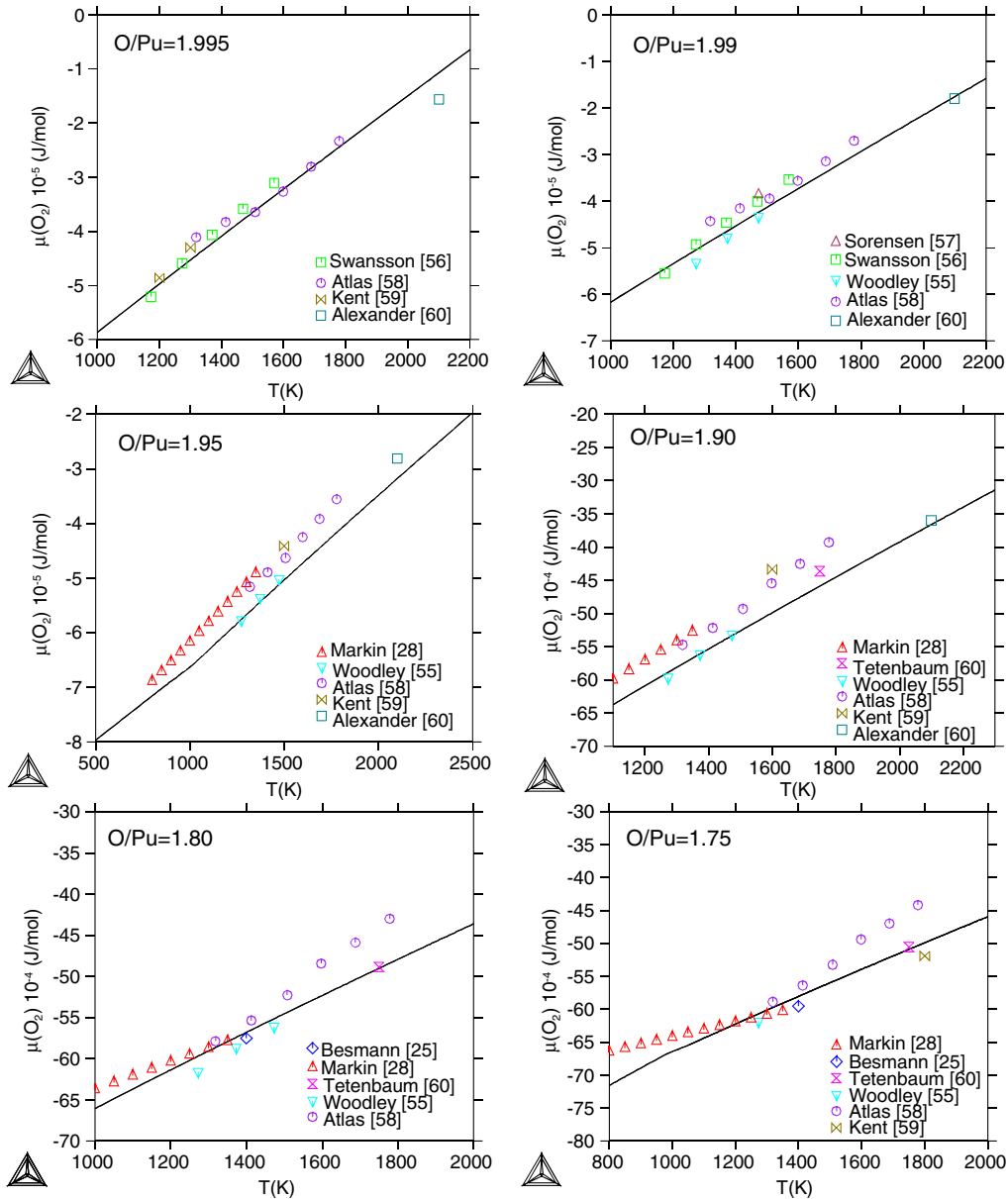
Fig. 10. Calculated partial Gibbs energy of O_2 as a function of temperature in PuO_{2-x} for fixed O/Pu ratios (present work) – comparison with available experimental data.

consistent with the fact that Glushko et al. [42] selected PuO_2 as the major species in the vapour over congruent PuO_{2-x} compound [42].

Finally, the total pressure and the partial pressures of Pu(g), PuO(g), PuO_2(g), O(g) and O_2(g) are calculated at 1970 K in Fig. 16 and compared to the curves reported by Ackermann et al. in [64]. Our results are in good agreement with the thermodynamic analysis performed by Ackermann et al. for the two-phase domain and for the PuO_{2-x} composition range [64]. The graph shows that PuO_2 heated at constant temperature under vacuum will start to loose O(g) and O_2(g). The rate of change of composition of the sample will be then quite large. Then PuO(g) and PuO_2(g) become more important and the rate of change of composition stops at the congruent composition where the total pressure is minimum (more exactly it is the flow of effusion that is minimum). Starting from the two-phase domain, the curve shows that the oxidation of $PuO_{1.61}$(s) is accomplished by the preferential vaporization of PuO(g).

Concerning the vaporization of Pu_2O_3–PuO_{2-x} and PuO_{2-x} systems, there is a good agreement between our thermodynamic

description based on the data of Glushko et al. [42] for the gas phase and the available experimental data on total pressures and congruent vaporization of PuO_{2-x}. In case of total pressure measurements, the authors have assumed the vapour to be PuO(g) above the two phase domain and PuO_2(g) above PuO_{2-x}. The partial pressures of PuO_2(g) and Pu(g) measured by Battles are not consistent with our calculations and with the values derived from the thermodynamic analysis of Ackermann et al. [64] and Glushko et al. [42]. Further investigations of the system by experiments or/and by calculations are required to clarify the situation especially the heat of formation and the heat capacity of Pu_2O_3.

5. Conclusion

In the framework of the FUELBASE project to develop a thermodynamic database for advanced fuels, a thermodynamic assessment of the whole plutonium–oxygen system is presented using the CALPHAD method considering the available experimental data reported in the literature. The compound energy formalism is used
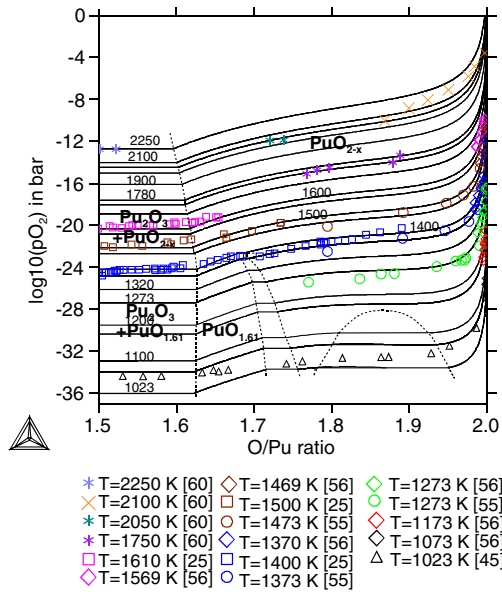
Fig. 11. Calculated O_2 partial pressure versus O/Pu ratio at 1023, 1073, 1100, 1173, 1200, 1273, 1320, 1373, 1400, 1470, 1500, 1570, 1600, 1688, 1750, 1780, 1900, 2000, 2050, 2100, 2250 K – comparison with the selected experimental data.
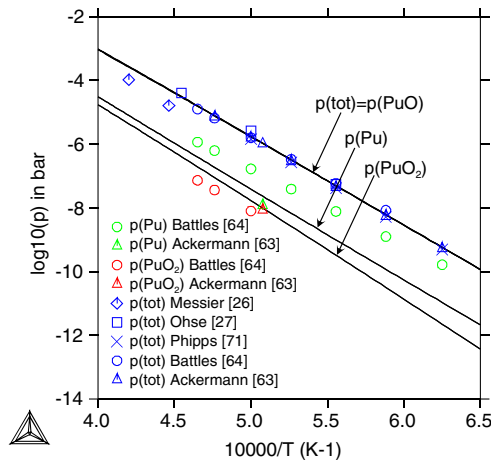

Fig. 12. Calculated PuO(g), Pu(g) and PuO_2(g) above the two-phase domain [$Pu_2O_3 + PuO_{2-x}$] (present work) – comparison with the available experimental data.

Fig. 13. Calculated congruent vaporization composition of PuO_{2-x} in both open and closed systems – comparison with the available experimental data for open system (effusion).

Fig. 14. Calculated total pressure versus the inverse of temperature for congruent effusion of PuO_{2-x} (present work) – comparison with the available experimental data for open system when PuO_2(g) is assumed to be the major species in the effused vapour.

Fig. 15. Calculated partial pressures of PuO(g) and PuO_2(g) versus reciprocal temperature for congruent vaporization of PuO_{2-x} in effusion cells (present work) – comparison with mass spectrometry data of Battles and Kent.

to describe the thermodynamic properties of the non stoichiometric oxide PuO_{2-x} and $PuO_{1.61}$ phases. The liquid phase is described using the ionic two-sublattice model. For the phase diagram, the experimental data selected by Wriedt [14] in his critical analysis have been adopted for the optimization. Concerning the experimental thermodynamic data, the oxygen partial Gibbs energy data are scattered. A chart has been built in order to compare the different set of data at fixed temperature or O/Pu ratio. The differences between the authors remain difficult to explain. A selection has been performed for the optimization. The main features of the phase equilibria between Pu_2O_3 and PuO_2 are well reproduced as well as the associated variation of the oxygen chemical potential versus temperature and composition. Using the present modelling of the condensed phases and the thermodynamic functions of the gaseous species from Glushko et al. [42], the vaporization behaviour of both two-phase Pu_2O_3–PuO_{2-x} domain and PuO_{2-x} monophasic region is studied. The total pressures and the congruent compositions calculated in both closed and open systems are well
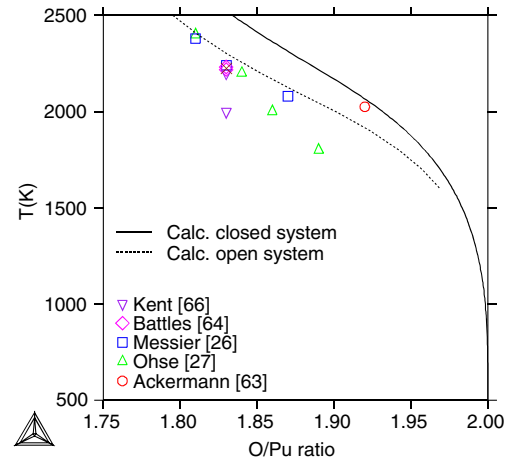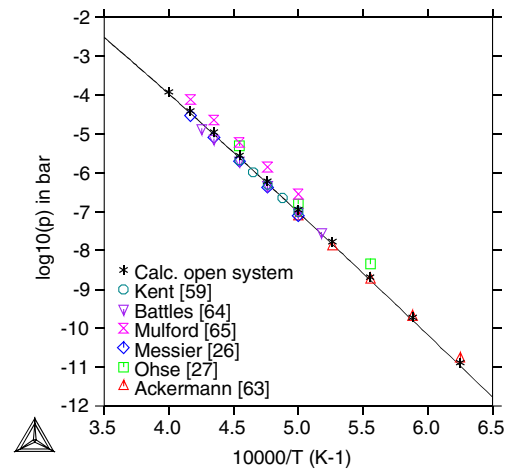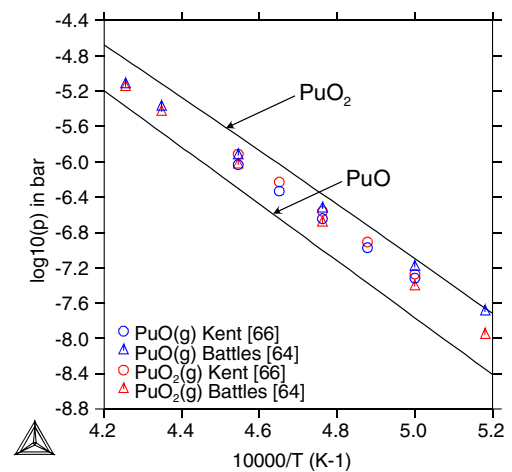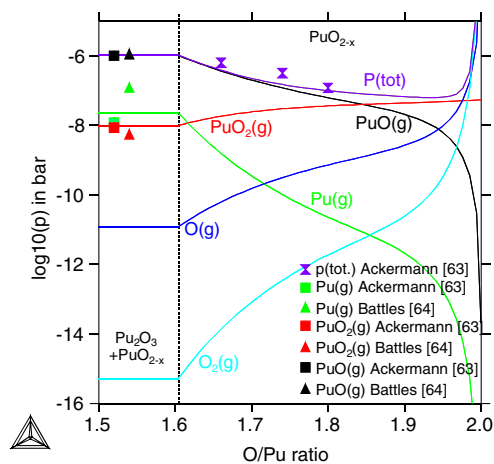
Fig. 16. Variation of the total and partial pressures versus O/Pu ratio at 1970 K for a closed system (present work) – the experimental data of Battles and Ackermann are reported for the two-phase domain.

reproduced. Difficulties remain to explain significant deviations between the experimental data on partial pressure measurements above the Pu_2O_3–PuO_2 and PuO_{2-x} systems. Experimental data are missing on the liquidus in the whole phase diagram and on the temperature range of stability of the $PuO_{1.61}$ phase in the Pu_2O_3–PuO_2 domain. Further experimental and/or theoretical work is required to establish the thermodynamic description of the Pu–O system. This remains fundamental work in order to model higher order systems such as U–Pu–O and U–Pu–MA–FP–O systems (MA = minor actinide, FP = fission product) to predict the behaviour of the fuel materials of the future fast breeder reactors.

Acknowledgements

References

[1] C. Guéneau, S. Chatain, J.C. Dumas, J. Lechelle, C. Rado, F. Defoort, N. Dupin, B. Sundman, H. Noel, R. Konings, in: Proceedings HTR 2006, Third International Topical Meeting on High Temperature Reactor Technology, 1–4 October, 2006, Johannesburg, South Africa.
[2] C. Guéneau, S. Chatain, S. Gossé, C. Rado, O. Rapaud, J. Lechelle, J.C. Dumas, C. Chatillon, J. Nucl. Mater. 344 (2005) 191.
[3] N. Saunders, A.P. Miodownik, CALPHAD, Calculation of Phase Diagrams, A Comprehensive Guide, Pergamon Materials Series, R.W. Cahn (Series Ed.), 1998.
[4] T.M. Besmann, T. Lindemer, J. Nucl. Mater. 130 (1985) 489.
[5] T.M. Besmann, T. Lindemer, J. Nucl. Mater. 137 (1986) 292.
[6] A. Nakamura, J. Nucl. Mater. 201 (1993) 17.
[7] M. Stan, P. Cristea, J. Nucl. Mater. 344 (2005) 213.
[8] H. Kinoshita, M. Uno, S. Yamanaka, J. Alloy Compd. 354 (2003) 129.
[9] M. Zinkevich, D. Djurovic, F. Aldinger, Solid State Ionics 177 (2006) 989.
[10] C. Guéneau, M. Baichi, D. Labroche, C. Chatillon, B. Sundman, J. Nucl. Mater. 304 (2002) 161.
[11] C.E. Holley, R.N. Mulford, E.J. Huber, E.L. Head, F.H. Ellinger, C.W. Bjorklund, Proc. Second United Nations Int. Conf. Peaceful Uses Atomic Energy 6 (1958) 215.
[12] T.D. Chikalla, C.E. McNeilly, R.E. Skavdahl, J. Nucl. Mater. 12 (2) (1964) 131.
[13] A.E. Martin, F.C. Mrazek, USAEC, Argonne Nat. Lab., Rep. ANL-7575, 1969.
[14] H.A. Wriedt, Bull. All. Ph. Dia., 11 (2), 1990, 184–202.
[15] W.H. Zachariasen, F.H. Ellinger, Acta Crystallogr. 16 (1963) 777.
[16] W.H. Zachariasen, F.H. Ellinger, Acta Crystallogr. 16 (1963) 369.
[17] W.H. Zachariasen, F.H. Ellinger, Acta Crystallogr. 8 (1955) 431433.
[18] F.H. Ellinger, Trans. Am. Inst. Min. Metall. Petrol. Eng. (Trans. AIME) 206 (1956) 1256.
[19] M. Wulff, G.H. Lander, J. Chem. Phys. 89 (5) (1988) 3295.
[20] J.C. Boivineau, J. Nucl. Mater. 60 (1976) 31.
[21] C. Sari, U. Benedict, H. Blank, Thermodynamics of Nuclear Materials, 1967, IAEA, Vienna (1968), pp. 587–611.
[22] D. Taylor, Trans. J. Brit. Ceram. Soc. 83 (1984) 32.
[23] E.R. Gardner, T.L. Markin, R.S. Street, J. Inorg. Nucl. Chem. 27 (1965) 541.
[24] G. Dean, J.C. Boivineau, P. Chereau, J.P. Marcon, Comm. Energ. Atom. Fr., Rep. CEA-CONF-701001-13, 1970.
[25] T. Besmann, J. Nucl. Mater. 144 (1987) 141.
[26] D.R. Messier, J. Am. Ceram. Soc. 51 (12) (1968) 710.
[27] R.W. Ohse, C. Ciani, Thermodynamics of Nuclear Materials, 1967, IAEA, Vienna (1968), pp. 545–557.
[28] T.L. Markin, A.J. Walter, R.J. Bones, Report AERE – R 4608, 1964.
[29] B. Riley, Sci. Ceram. 5 (1970) 83.
[30] L.E. Russel, Plutonium 1960, E. Grison, W.B.H. Lord, R.D. Fowler (Eds.), Cleaver-Hume, London, 1961, pp. 489–492.
[31] J.L. Drummond, G.A. Welsh, J. Chem. Soc. (1957) 4781.
[32] E.E Jackson, M.H. Rand, Report AERE – R 3636, 1963.
[33] J.M. Haschke, T.H. Allen, J. Alloys Compd. 336 (2002) 124.
[34] V. Neck, M. Altmaier, T. Fanghänel, J. Alloy Compd. 444&445 (2007) 464.
[35] P. Martin, S. Grandjean, M. Ripert, M. Freyss, P. Blanc, T. Petit, J. Nucl. Mater. 320 (2003) 138.
[36] J.D. Farr, R.K. Schulze, M.P. Neu, J. Nucl. Mater. 328 (2004) 124.
[37] S.D. Conradson, B.D. Begg, D.L. Clark, C. den Auwer, M. Ding, M.; P.K. Dorhout, F.J. Espinosa-Faller, P.L. Gordon, R.G. Haire, N.J. Hess, R.F. Hess, D.W. Keogh, L.A. Morales, M.P. Neu, P. Paviet-Hartmann, W. Runde, C.D. Tait, D.K. Veirs, P.M. Villella, J. Am. Chem. Soc. 126 (41) (2004) 13443.
[38] L. Petit, A. Svane, Z. Szotek, W.M. Temmerman, Science 301 (2003) 498.
[39] P.A. Korzhavyi, L. Vitos, D.A. Andersson, B. Johansson, Nat. Mater. 3 (2004) 225.
[40] E.A. Aitken, S.K. Evans, USAEC, General Electric, Vallecitos Nucleonics Lab., Rep. GEAP-5672, 1968.
[41] H.E. Flotow, M. Tetenbaum, J. Chem. Phys. 74 (9) (1981) 5269.
[42] V.P. Glushko, L.V. Gurvich, G.A. Bergman, I.V. Veits, V.A. Medvedev, G.A. Khachakuruzov, V.S. Yungman, Thermodyn. Prop. Individual Subs. 4 (1982) 231 (Nauka, Moscow).
[43] R.J. Lemire, J. Fuger, H. Nitsche, P. Potter, M.H. Rand, J. Rydberg, K. Spahiu, J.C. Sullivan, W.J. Ullman, P. Vittorge, H. Wanner, in: Chemical Thermodynamics of Neptunium and Plutonium, vol. 4, Edited by OECD Nuclear Energy Agency, Elsevier, 2001, pp. 331–338.
[44] I. Ansara, B. Sundman, Scientific group thermodata Europe, in: P.S. Glaser (Ed.), Computer Handling and Determination of Data, North Holland, Amsterdam, 1986, p. 154.
[45] T.L. Markin M.H. Rand, Thermodynamics, vol. 1, IAEA, Vienna, 1966, pp. 145–156.
[46] P. Chereau, G. Dean, M. De Franco, P. Gerdanian, J. Chem. Thermodyn. 9 (1977) 211.
[47] T.A. Sandenaw, J. Nucl. Mater. 10 (3) (1963) 165.
[48] O.L. Kruger, H. Savage, J. Chem. Phys. 49 (10) (1968) 4540.
[49] T.K. Engel, J. Nucl. Mater. 31 (1969) 211.
[50] A.E. Ogard, Plutonium 1970 and other actinides, Nuclear Metallurgy, vol 17, No. 1, W.N. Miner (Ed.), Metall. Soc. AIME, Warrendale, PA, 1970, pp. 78–83.
[51] F.L. Oetting, J. Nucl. Mater. 105 (1982) 257.
[52] R.J.M. Konings, D. Sedmidubsky, Rep. JRC-ITU-TN-2005/20, 2005.
[53] M.M. Popov, M.I. Ivanov, Sov. J. At. Energy 2 (4) (1957) 439.
[54] G.K. Johnson, E.H. Van Deventer, O.L. Kruger, W.N. Hubbard, J. Chem. Thermodyn. 1 (1969) 89.
[55] R.E. Woodley, J. Nucl. Mater. 96 (1981) 5.
[56] G.C. Swansson, USAEC, Los Alamos Sci. Lab., Rep. LA-6083-T, 1975.
[57] O.T. Sorensen, Plutonium 1975 and other actinides, H. Blank, R. Lindner (Eds.), North-Holland, Amsterdam, 1976, pp. 123–131.
[58] L.M. Atlas, G.J. Schlehman, Plutonium 1965, A.E. Kay, M.B. Waldron (Eds.), Chapman and Hall, London, 1967, pp. 845–857.
[59] R.A. Kent, R.W. Zocher, USAEC, Los Alamos Sci. Lab. Rep. LA-6534, 1976.
[60] M. Tetenbaum, Plutonium Chemistry, Am. Chem. Soc. Symp. Ser. 216, Am. Chem. Soc., Washington, 1983, pp. 109–122.
[61] D. Labroche, O. Dugne, C. Chatillon, J. Nucl. Mater. 312 (2003) 21.
[62] M. Baïchi, C. Chatillon, G. Ducros, K. Froment, J. Nucl. Mater. 349 (2006) 17.
[63] T.E. Phipps, G.W. Sears, O.C. Simpson, J. Chem. Phys. 18 (5) (1950) 724.
[64] R.J. Ackermann, R.L. Faircloth, M.H. Rand, J. Phys. Chem. 70 (1966) 3698.
[65] J.E. Battles, J.W. Reihus, W.A. Shinn, USAEC, Argonne Nat. Lab., Rep. ANL-7575, 1969.
[66] R.N.R. Mulford, C.E. Holley, USAEC, Los Alamos Sci. Lab. Rep. LA-DC-8266, 1966.
[67] R.A. Kent, Report LA-5202-MS, March, 1973.
[68] O.H. Krikorian, A.S. Fontes, B.B. Ebbinghaus, M.G. Adamson, J. Nucl. Mater. 247 (1997) 161.
[69] C. Ronchi, F. Capone, J.Y. Colle, J.P. Hiernaut, J. Nucl. Mater. 280 (2000) 111.
[70] B. Jansson, Report TRITA-MAC-0234, Royal Institute Technology, S10044 Stockholm 70, Sweden, April 1984.
[71] B. Sundman, B. Jansson, J.O. Andersson, Calphad 9 (1985) 153.
[72] A. Dinsdale, Calphad 15 (1991) 317.
[73] A.N. Grundy, E. Povoden, T. Ivas, L.J. Gauckler, Comp. Coup. Ph. Diag. Thermoch. 30 (2006) 33.
[74] M. Hillert, B. Jansson, B. Sundman, J. Agren. Metall. Trans. A 16 (1985) 661.